https://doi.org/10.1070/RCR4973

# Modern bio and chemical sensors and neuromorphic devices based on organic semiconductors

**Polina A. Shaposhnik,[a, b] Sergey A. Zapunidi,[b] Mikhail V. Shestakov,[b] Elena V. Agina,[b] Sergey A. Ponomarenko [a, b]***

*[a] Department of Chemistry, Lomonosov Moscow State University, Leninskie Gory 1, stroenie 3, 119991 Moscow, Russian Federation*
*[b] Enikolopov Institute of Synthetic Polymeric Materials, Russian Academy of Sciences, ul. Profsoyuznaya 70, 117393, Moscow, Russian Federation*

This review summarizes and highlights the current state-of-the-art of research on chemical sensors and biosensors in liquid environment and neuromorphic devices based on electrolyte-gated organic transistors with the active semiconductor layer of organic π-conjugated materials (small molecules, oligomers and polymers). The architecture and principles of operation of electrolyte-gated organic transistors and the main advantages and drawbacks of these devices are considered in detail. The criteria for the selection of organic semiconductors for these devices are presented. The causes of degradation of semiconductor layers and ways of their elimination are discussed. Examples of the use of electrolyte-gated organic transistors as bio and chemical sensors, artificial synapses and computing devices are given.
The bibliography includes 132 references.

## Contents

1. Introduction 1483
2. Architecture and operation mechanisms of electrolyte-gated organic transistors 1485
3. Materials for electrolyte-gated organic transistors 1488
   3.1. Materials for semiconductor layers 1488
   3.2. Materials for electrodes and substrates 1492
4. Operation stability of electrolyte-gated organic transistors 1492
5. Application of electrolyte-gated organic transistors 1496
   5.1. Biosensors 1496
   5.2. Chemical sensors 1500
   5.3. Neuromorphic devices 1501
6. Conclusion 1504

## 1. Introduction

The following abbreviations are used in the review:

AFM — atomic force microscopy,
BPA — bisphenol A,
BSA — bovine serum albumin,
CRP — C-reactive protein,
EDL — electric double layer,
EGOFET — electrolyte-gated organic field-effect transistor,
EGOT — electrolyte-gated organic transistor,
IL-6 — interleukin-6,
ISFET — ion-sensitive field-effect transistor,
ISM — ion-selective membrane,
MOSFET — metal-oxide-semiconductor field-effect transistor,
NOMFET — nanoparticle organic memory field-effect transistor,
NPs — nanoparticles,
OECT — organic electrochemical transistor,
OFET — organic field-effect transistor,
P3HT — poly(3-hexylthiophene),
PCBM — phenyl-C61-fullerene butyric acid methyl ester,
PCT — procalcitonin,
PEDOT : PSS — poly(3,4-ethylenedioxythiophene)/poly(styrene sulfonic acid) complex,
SEM — scanning electron microscopy,
TEG — triethylene glycol,
TNF — tumour necrosis factor,
XPS — X-ray photoelectron spectroscopy.

**Symbols of physical quantities**:

$E$ — electric field in the conducting channel,
$C_i$ — capacitance per unit area,
$I_{ds}$ — drain – source current,
$I_{ds\ lin}$ — drain – source current in the linear regime,
$I_{ds\ sat}$ — drain – source in the saturation regime,
$I_{gs}$ — gate – source current (leakage current),
$I_{on/off}$ — on/off current ratio,
$i_s$ — ionic strength of the solution,
$L$ — length of the conducting channel,
$V_{ds}$ — drain – source voltage,
$V_{gs}$ — gate – source voltage,
$V_t$ — threshold voltage,
$Q$ — charge density per unit area in the conducting channel,
$W$ — width of the conducting channel,
$\lambda$ — Debye screening length,
$\mu$ — charge carrier mobility,
$\mu_{lin}$ — charge carrier mobility in the linear regime,
$\mu_{sat}$ — charge carrier mobility in the saturation regime.

There is a growing demand for new biological and chemical sensors all over the world. Such devices allow the detection of biological entities and chemical compounds in

**Received 22 June 2020**
© 2020 Uspekhi Khimii, ZIOC RAS, Russian Academy of Sciences and IOP Publishing Limited

solutions through the interaction with a recognition element and the determination of the analyte concentrations by measuring the electrical conductivity of solutions, their optical spectra and so on.[1] Sensors can be divided into two types according to the principle of construction. Sensors of one type are sophisticated stationary instruments operated by skilled personnel.[1] Usually, these instruments are employed in research laboratories, hospitals or centres of expertise. Sensors of another type are portable devices for rapid in-field analysis suitable for use in households, such as the control of the blood glucose levels, pregnancy tests, the testing for drug or alcohol intoxication and so one. This group of sensors includes two types of organic electronic devices — organic electrochemical transistors (OECT)[2] and electrolyte-gated organic field-effect transistors (EGOFET),[1,3] which can be considered under the common name of electrolyte-gated organic transistors (EGOT).

The ion-sensitive field-effect transistor (ISFET) invented by P.Bergveld in 1970[4,5] can be considered as the parent of electrolyte-gated transistors. The main goal of Bergveld's research was to design a new portable fast sensor suitable for ion activity measurements in small liquid volumes. The ISFET was based on a metal-oxide-semiconductor field-effect transistor (MOSFET). Later, the surface modification of gate electrodes with enzymes or antibodies[6] has significantly expanded the area of application of ISFET sensors and stimulated the progress in biosensors. The current state-of-the-art of research on ISFET-based biosensors and their use in *in vitro* diagnostics are considered in the review by Sakata.[7]

In EGOT-based sensors, change in the analytical signal (changes in the threshold voltage, charge carrier mobility, drain – source current, transconductance) is induced by the interaction between the analyte and the chemical or biological recognition layer deposited on the surface of an organic semiconductor or gate. Advantages of EGOT sensors are that they are label-free, *i.e.*, they do not require the introduction of an optical or electroactive probe conjugated with the analyte.[1,8–11] A picomolar limit of detection of analytes by EGOT-based sensors was reported in a number of publications.[10,12,13] Hence, these sensors can be employed in clinical practice. Besides, lower limits of detection were achieved in other studies.[14,15] Therefore, methods using EGOT-based sensors may compete with immunoenzymatic assays (enzyme-linked immunosorbent assay, ELISA) as a diagnostic method.[16–18] Electrolyte-gated organic transistors can be fabricated using printing technologies, which significantly reduces the manufacturing cost of EGOTs.[19,20]

Electrolyte-gated organic transistors are of great interest for use as artificial synapses. In biology, a synapse is a point of contact between two neurons or between a neuron and another cell, where the transmission of a nerve impulse occurs.[21] Electrolyte-gated organic transistors were proposed to use as prostheses to restore synaptic contacts[22] or as devices for investigation of neural activity.[23,24] Besides, EGOTs can be utilized as memory elements for neuromorphic computing systems.[25,26] Traditional computers are based on the von Neumann architecture, and their operation rate is limited by the data transfer rate between the random-access memory (RAM) and the central processing unit (CPU).[27] In neuromorphic computing systems, computing elements and memory are fused together. This makes it possible to overcome the limitation associated with the data transfer rate and finally to construct an artificial neural network.[21,28]

In 2010, Horowitz and co-workers[29] were among the first who used pure water as an electrolyte gate in a field-effect transistor. Since that time, the number of publications on this issue has been gradually increasing. Several reviews on this subject are currently available.[1,3,20,30,31] The review by Torsi *et al.*[1] is for informational purposes and is useful for researchers who have just started their work on sensors based on organic transistors. The review by Cramer *et al.*[3] is devoted to water-gated OFETs, materials for their fabrication, physical and electrochemical principles of operation and application of these OFETs as biological sensors and for the stimulation of electrical activity of neurons. In 2016, Piro and co-workers[30] summarized the data on the application of EGOTs as biosensors published in the previous five years. Picca *et al.*[20] analyzed the performance of EGOFETs and OECTs as biosensors, with the focus on the role of Faradaic processes and interactions at the electrolyte/semiconductor interface. Manoli *et al.*[32] considered applications of EGOTs fabricated by printing technologies in bioelectronics. In the mini review, Liao *et al.*[31] considered biological and chemical sensors based on OECTs with the poly(3,4-ethylenedioxythiophene)/poly(styrene sulfonic acid) complex (PEDOT : PSS) as the semiconductor layer and summarized methods of surface modification of semiconductors and gates in these devices.

**P.A.Shaposhnik**. PhD student at the Department of Chemistry of the MSU, Junior Researcher at the ISPM RAS.
E-mail: polinashaposhnik@ispm.ru
*Current research interests*: biosensors based on electrolyte-gated organic transistors, electronic tongue systems, design of stable semiconductor materials for water environment, development of methods for the deposition of thin films for application in aqueous environment.
**S.A.Zapunidi**. PhD in Physics and Mathematics, Researcher at the ISPM RAS.
E-mail: zap@physlab.ru
*Current research interests:* semiconducting polymers, electronic devices, lab-on-a-chip, nanotechnology.
**M.V. Shestakov**. PhD in Physics, Junior Researcher at the ISPM RAS.
E-mail: shestakovmv@ispm.ru
*Current research interests:* doped zinc oxide nanoparticles for solar light conversion; oxyfluoride glasses for stained glass windows and lasers; bio and chemical sensors based on semiconductor transistors.
**E.V.Agina**. Doctor of Chemical Sciences, Leading Researcher at the ISPM RAS. E-mail: agina@ispm.ru
*Current research interests:* molecular and supramolecular self-assembly in the bulk and thin films of linear and branched carbosilane-siloxanes with various functionalities, in particular with mesogenic and semiconducting groups; development of efficient methods for the fabrication of highly organized (two-dimensional) nanomaterials with the predetermined structure and properties based on carbosilane-siloxanes.
**S.A.Ponomarenko**. Corresponding Member of the Russian Academy of Sciences, Doctor of Chemical Sciences, Director of the ISPM RAS, Professor of the MSU. E-mail: ponomarenko@ispm.ru
*Current research interests:* molecular design and synthesis of new conjugated organic and organosilicon structures, primarily based on thiophene and silicon chemistry, with high charge carrier mobility, efficient luminescence, good processability in solution, oxidative and thermal stability and other properties required for the creation of promising materials and technologies for organic electronics and photonics.

Translation: T.N.Safonova

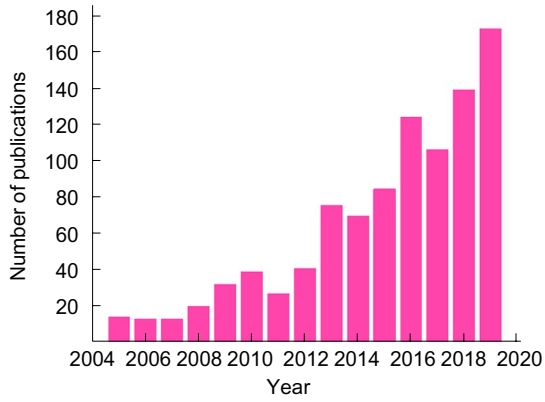



**Figure 1.** Evolution of the overall number of publications on the subjects 'electrolyte-gated organic transistors' and 'organic electrochemical transistor' per year over the past 15 years in the database Web of Science.

Meanwhile, a large number of new studies of EGOTs, with a significantly growing range of applications, were reported after the publication of the latest review (Fig. 1). Electrolyte-gated organic transistors were applied as biological [11] and chemical sensors,[33] artificial synapses [22] and in computing devices.[25]

The goal of this review is to briefly describe the principles of operation of EGOFETs and OECTs, consider materials used for their fabrication, analyze the factors responsible for the degradation of the manufactured devices and highlight the most promising areas of their practical applications.

The review includes five sections. The Introduction is followed by the detailed consideration of the architecture of EGOFETs and OECTs, their similarity and differences and the physical principles of operation. The next section is devoted to the criteria for the selection of materials, in particular organic semiconductors, electrodes and substrates, for the use in EGOTs. After that, the factors responsible for the degradation of EGOTs and methods for prevention of degradation are discussed. In the final section, the prime examples of the application of EGOTs as biological and chemical sensors and neuromorphic devices are given.

## 2. Architecture and operation mechanisms of electrolyte-gated organic transistors

The term 'electrolyte-gated organic transistor' combines two types of devices with similar architecture but different operation mechanisms, namely, electrolyte-gated organic field-effect transistors and organic electrochemical transistors.

Both types of devices consist of an organic semiconductor layer over a non-conducting substrate and conducting contacts — drain and source electrodes and a gate electrode separated from the semiconductor by the electrolyte layer (Fig. 2 *a*). Generally, a small amount of a liquid electrolyte is placed in a special reservoir, which is mounted on the semiconductor surface, or a solid electrolyte layer (polymer,

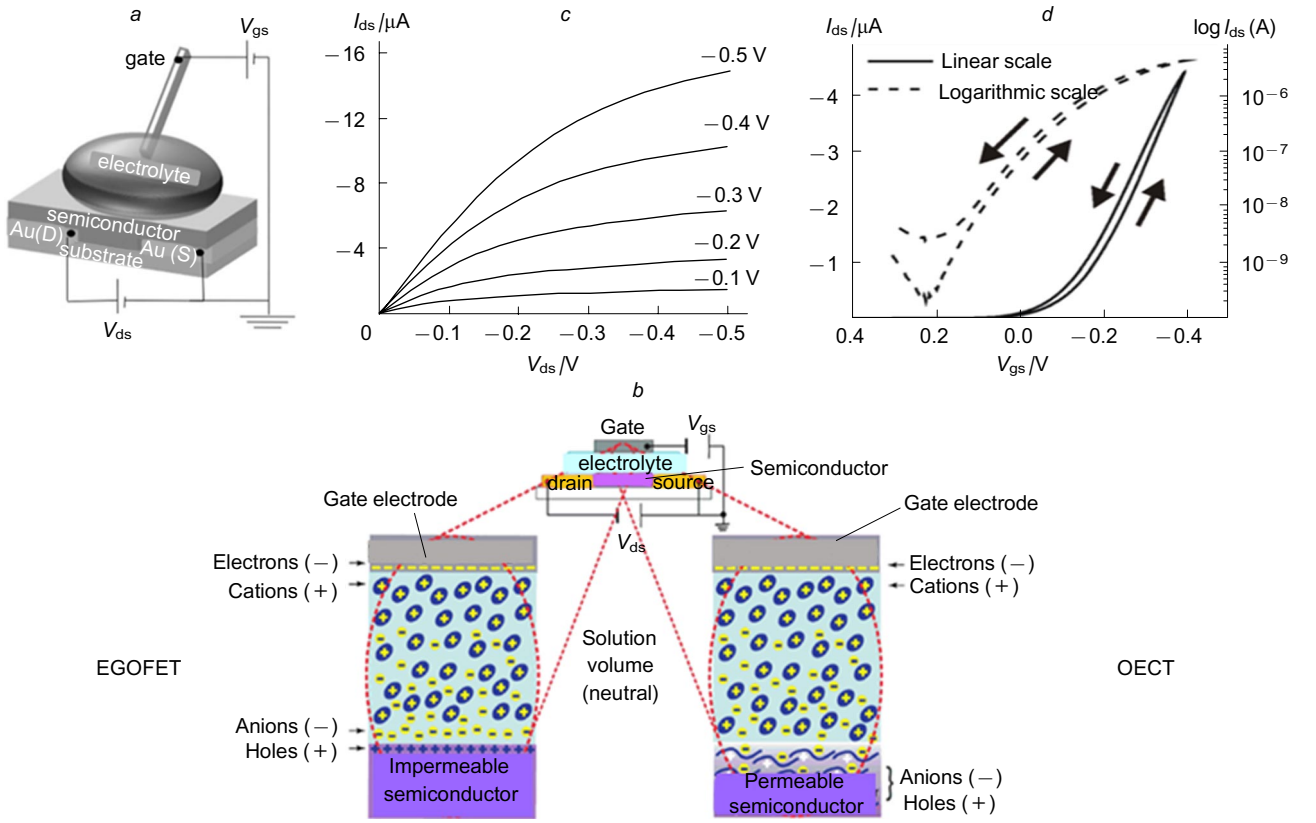



**Figure 2.** Schematics of an electrolyte-gated transistor (*a*);[29] operation mechanisms of EGOFETs and OECTs (*b*),[34] the output (*c*) and transfer (*d*) $I-V$ curves.[35]
$V_{gs}$ is the gate – source voltage, $V_{ds}$ is the drain – source voltage, $I_{ds}$ is the drain – source current. Hereinafter, the polarity of the power supplies is the same as that presented in the figures in the original publications.

ionic liquid or ionic gel) is deposited on the semiconductor surface.[30, 36–39] Then the gate electrode is immersed in the electrolyte layer; in the case of a solid electrolyte, the gate electrode is deposited by vacuum evaporation or magnetron sputtering.[39–41] The main difference in the architecture of EGOTs and OFETs is that conducting solutions or a solid electrolyte are utilized in EGOTs instead of a solid dielectric layer employed in traditional organic field-effect transistors (OFETs).[42]

The operation of EGOTs is based on the same principle as that of conventional OFETs. When discussing the operation of EGOTs, it is worth noting that, although non-doped organic semiconductor materials are ambipolar (*i.e.*, they are capable of hosting both hole and electron conduction depending on the work function of contacts in the device), only one contact material (generally gold) is used in most experiments. Consequently, an organic semiconductor can show either p- or n-type behaviour. Hence, hereinafter these terms are used implying that the organic semiconductor behaves as a semiconductor of a particular type in the device under consideration. Most of semiconductor materials employed in organic electronics exhibit hole conduction when combined with gold contacts. Therefore, this section deals with p-type organic transistors. It should be noted that n-type transistors based on electron transporting (n-type) organic semiconductors operate in a similar fashion with the exception that the drain–source voltage ($V_{ds}$) for such transistors should have a positive value. Note that these materials are less commonly utilized in EGOTs, because they are (with rare exceptions) less stable in air and in the presence of an electrolyte.[39]

When no voltage is applied to the gate electrode, only a very weak electric current can flow from the source to the drain through the organic semiconductor due to the intrinsic conductivity of the semiconductor, which is very low (in this case, we do not consider doped semiconductors). When the voltage $V_{gs} < 0$ V is applied to the gate of OFET (in a standard configuration, the voltage is measured relative to the grounded source contact [1]), the dielectric is polarized and free charge carriers (holes) in the semiconductor begin to move towards the semiconductor/dielectric interface to compensate the equivalent charge at the gate/dielectric interface. This gives rise to a conducting channel at the semiconductor/dielectric interface. The voltage at the gate needed to create the conducting channel is called the threshold voltage (hereinafter $V_t$). If a negative voltage is applied to the drain and source contacts, the holes are injected from the source electrode and start to move within the current-conducting channel.[43]

In the case of an electrolyte-gated p-type transistor, the application of a negative voltage to the gate electrode immersed in an electrolyte solution leads to the accumulation of cations at the gate/electrolyte interface and of anions at the organic semiconductor/electrolyte interface. The accumulation of ions results in the formation of electric double layers (EDLs) at the semiconductor/electrolyte and electrolyte/gate interfaces.[1, 34, 35, 44] These EDLs, the capacitance of which reaches tens of microfarads per square centimetre for water and aqueous solutions,[35, 45] are considered as plates of the capacitor, at which the charge is accumulated. Due to a high capacitance of such capacitors, EGOTs can operate at voltages of $<1$ V, which is significantly lower than the voltage required for the operation of OFETs. Generally, the specific capacitance of OFETs is tens of nanofarads per square centimetre.[2] Hence, the electrical resistance of the current-conducting channel in both EGOTs and OFETs can be controlled by changing the voltage at the gate electrode, but using significantly lower operation voltages in case of EGOT.

The operation mechanisms of EGOFETs and OECTs differ in that the charge migration in the current-conducting channel in EGOFETs (like in OFETs) occurs only due to the applied electric field. In OECTs, the applied electric field induces also reversible injection of ions from the electrolyte layer to the semiconductor layer (Fig. 2 *b*); *i.e.*, the operating OECT has two types of charge carriers. Colucci *et al.*[46] stated that this is accompanied by a redox reaction described by the following relation (for anions and a polymeric semiconductor):

$$P^0 + Z^- \rightleftharpoons P^+Z^- + e \quad (1)$$

where $P^0$ is an active polymer, $Z^-$ are anions and e is an electron. It should be emphasized that the threshold voltage in OECTs corresponds to the potentials of the oxidation or reduction reaction of the organic semiconductor that occurs upon ion adsorption. It should be noted that the operation mechanisms of EGOFETs and OECTs can be divided rather arbitrarily. It was reported [47] that EGOTs based on certain organic semiconductor materials can operate as EGOFETs at low voltages and as OECTs at higher voltages due apparently to rather high redox potentials of these materials.

Shockley approximation developed for MOSFETs is commonly applied to describe EGOFETs and OECTs, as well as OFETs. This approximation relies on the assumption that the charge carrier density associated with the electric field change along the transistor channel is much lower than the charge density associated with the electric field change in the bulk of the channel, *i.e.*,

$$\left|\frac{\partial F_x}{\partial x}\right| \ll \left|\frac{\partial F_y}{\partial y}\right| \quad (2)$$

where $F$ is the electric field, $x$ is the direction parallel to the insulator/semiconductor interface and $y$ is the direction perpendicular to this interface.[48] Condition (2) is met if the channel length ($L$) is much larger than the thickness of the insulator $d_i$ [generally, $L > 10\,d_i$ (Ref. 49)].

Another assumption is that the charge mobility ($\mu$) is independent of the applied field. Actually, at high drain–gate voltages, the charge mobility can display the dependence on the voltage.[48] The specific dielectric capacitance ($C_i$) is also taken to be constant although, in the case of EGOTs, the situation is more complex because the device contains two EDLs rather than a single solid dielectric and the EDL capacitance is affected by the ionic strength of the solution. Thus, Cramer *et al.*[35] used a 0.1 M NaCl solution and measured the specific capacitance, which was found to be 14.6 and 7.8 μF cm$^{-2}$ for EDL and pure water, respectively. Therefore, it is necessary to take into account the ionic strength of the solution when calculating the parameters of the device.

The third condition for the application of Shockley approximation is the absence of the leakage current in the device, *i.e.*, the gate–drain current $I_{gs}$ should be equal to zero. Actually, leakage currents are always present, but these currents should be much smaller that the drain–source current $I_{ds}$ for the correct performance of the device (generally, the difference of three orders of magnitude is

thought to be acceptable). Besides, the potential barrier for the charge carrier injection from the electrode to the semiconductor, which is responsible for the contact resistance in the device, should be as small as possible. In practice, this is achieved by choosing a material for the electrode such that the work function of the electrode would be close to the corresponding electron levels of the semiconductor. Despite these assumptions and limitations on the performance of the device in order to achieve the consistency with Shockley approximation, the mathematical model of this approximation adequately describes the current-voltage characteristics ($I-V$ curves)† of both EGOFETs and OECTs.

Let us consider the main equation describing the voltage dependence of the current $I_{ds}$ in Shockley approximation.[49] If the $V_{gs}$ value is larger than the threshold voltage $V_t$, the density of injected charge carriers per unit area ($Q$) can be calculated as follows:

$$Q = C_i(V_{gs} - V_t) \tag{3}$$

where $C_i$ is the dielectric capacitance per unit area. Equation (3) is written for the semiconductor film at a point in the vicinity of the source, the potential of which is equal to zero. In the general case, the density of injected charges at the point with the coordinate $x$, calculated with respect to the source, depends also on the potential $V(x)$, which is determined by the voltage at the drain. Hence, Eqn (3) takes the following form:

$$Q = C_i(V_{gs} - V_t - V(x)) \tag{4}$$

If the charge carrier diffusion is ignored and only the charge motion induced by the electric field is considered, the current in the transistor channel created by injected charges as a function of their density $Q$ can be described as follows:

$$I_{ds} = W\mu QE_x \tag{5}$$

where $W$ is the channel width and $E_x$ is the electric field along the $x$ axis. By applying the above-mentioned Shockley condition for two-dimensionality of the conducting channel, $E_x$ can be expressed as follows

$$E_x = \frac{dV}{dx} \tag{6}$$

From Eqn (5), taking into account Eqn (6), we derive

$$I_{ds}\,dx = W\mu C_i(V_{gs} - V_t - V(x))\,dV \tag{7}$$

To determine the total current in the channel, it is necessary to integrate Eqn (7) along the coordinate $x$ from zero (the position of the source) to $L$ (the position of the drain); in this case, $V(x)$ varies from zero to $V_{ds}$. Assuming that the values of $\mu$ and $C_i$ are independent of the charge carrier density and, consequently, of the voltage at the gate, the following general expression for the drain – source current can be derived

$$I_{ds} = \mu\frac{WC_i}{L}\left[(V_{gs} - V_t)V_{ds} - \frac{V_{ds}^2}{2}\right] \tag{8}$$

There are two operating regimes of organic transistors — linear and saturation. At low voltages, the drain – source current $I_{ds}$ obeys the Ohm law and is proportional to $V_{ds}$ at a fixed gate – source voltage. From Eqn (8), by neglecting the quadratic term, one can derive the equation for the current in the conducting channel in the linear regime

$$I_{ds\,lin} = \mu_{lin}\frac{WC_i}{L}(V_{gs} - V_t)V_{ds} \tag{9}$$

The criterion of the applicability of the linear regime is based on the relation

$$V_{ds} \ll (V_{gs} - V_t) \tag{9a}$$

Differentiation of Eqn (9) with respect to $V_{gs}$, with $V_{ds}$ assumed to be constant, gives the following equation for the determination of the charge mobility in the linear regime

$$\mu_{lin} = \frac{L}{WC_iV_{ds}}\frac{dI_{ds}}{dV_{gs}} \tag{10}$$

The $V_{ds}$ potential difference becomes too large compared to $V_{gs}$ with increasing magnitude of the drain – source voltage. There comes a moment when the region in the vicinity of the source becomes depleted of positive charges. In this case, the channel current is limited to $I_{ds\,sat}$. Hence, when the relation is satisfied

$$V_{ds} > (V_{gs} - V_t) \tag{11}$$

the channel current is described by the following equation

$$I_{ds\,sat} = \mu_{sat}\frac{WC_i}{2L}(V_{gs} - V_t)^2 \tag{12}$$

The threshold voltage $V_t$ and the charge mobility in the saturation regime ($\mu_{sat}$) are evaluated from the plot of the square root of the current in the saturation regime *versus* the gate voltage. This dependence is described by the following equation

$$\sqrt{I_{ds\,sat}} = \left(\mu_{sat}\frac{WC_i}{2L}\right)^{1/2}(V_{gs} - V_t) = AV_{gs} - B \tag{13}$$

From which we deduce

$$\mu_{sat} = \frac{2L}{WC_i}A^2 \tag{14}$$

$$V_t = -\frac{B}{A} \tag{15}$$

The on/off current ratio $I_{on/off}$, calculated by the ratio of the maximum channel current to the current in the off state, is another parameter for the evaluation of the performance of the field-effect transistor. The ratio $I_{on/off}$ characterizes the ability of the device to switch between two conduction regimes.[1]

To avoid unwanted electrochemical reactions and the leakage current when working with EGOT, it is necessary to select the right voltage range. Pure water is a weak electrolyte with a conductivity of $\sim 10^{-3}$ S cm$^{-1}$ (Ref. 3). When

† The $I-V$ curve represent the current in the conducting channel of the transistor (drain – source current, $I_{ds}$) as a function of the voltage. There are the following two types of $I-V$ curves: output curves characterizing $I_{ds}$ as a function of the drain – source voltage ($V_{ds}$) at a fixed drain – gate voltage $V_{gs}$ (see Fig. 2 *c*) and transfer curves characterizing the dependence of $I_{ds}$ on $V_{gs}$ at a constant $V_{ds}$ (see Fig. 2 *d*).

picking the operating voltage range, one should take into account the possibility of the occurrence of the following redox processes in an aqueous solution:

$$H_2O \rightleftharpoons 2H^+ + 1/2\,O_2\uparrow + 2e \quad (16)$$

$$2H_2O + 2e \rightleftharpoons H_2\uparrow + 2OH^- \quad (17)$$

The standard potentials of the half-reactions measured with respect to the standard hydrogen electrode are 0.571 and −0.658 V, respectively.[3] However, the drain – source and drain – gate voltages, which are somewhat higher that the above values, are often used in practice.[50] This is due to the fact that EGOTs are fabricated taking measures to protect the drain and source contacts from direct exposure to aqueous solutions. The contacts are generally coated with a semiconductor layer[50 – 52] or a special passivating layer.[53, 54]

The above-considered mathematical model that describes processes in both OFET and EGOT can be used to calculate such parameters as the threshold voltage, the charge mobility and the transconductance from the measured output and transfer CVCs

$$g_m = \frac{dI_{ds}}{dV_{gs}} \quad (18)$$

Bio- or chemical sensors are fabricated by coating the surface of the semiconductor or the gate electrode with a layer of receptor molecules capable of specifically binding to analyte molecules and ions. Since the EDL width at the interface is at most a few angströms, a change in the morphology of the modified surface caused by the interaction with the analyte affects the charge movement in the conducting channel and leads to changes in the values of $V_t$, $\mu$ and $g_m$ (sensing mechanisms are considered in more detail in Section 5.1). Therefore, measurements of the $I-V$ curves of EGOTs containing a receptor layer provide data on the concentration of analyte species in solution. This process is not time-consuming, does not require high computational resources and can easily be automated.

## 3. Materials for electrolyte-gated organic transistors

### 3.1. Materials for semiconductor layers

The selection of a material and the choice of the technique for the deposition of a semiconductor layer are of great importance for the fabrication of EGOFETs and OECTs. The main requirements for the semiconductor layer in EGOFETs are the same as those for semiconductor layers in OFET and include high charge mobility and high on/off current ratio ratios. According to Zhang *et al.*,[36] $\mu$ of about 0.1 $cm^2\ V^{-1}\ s^{-1}$ is a groundbreaking performance characteristic for EGOFETs. The parameter $g_m$, which reaches tens of millisiemens, is more commonly used to characterize OECTs.[55, 56] Good values of $I_{on/off}$ for EGOFETs and OECTs are $10^3$ (Ref. 36) and $10^5 – 10^8$ (Refs 25 and 57), respectively.

Additional requirements are imposed on materials for EGOFETs compared to materials for OFETs. This is because in most cases the semiconductor in EGOFETs is in direct contact with the electrolyte, which causes accelerated degradation of the semiconductor layer. Electrochemical doping is the main cause of degradation.[30] Hence, electrochemical stability is one of criteria for the selection of a material for EGOFETs (causes of degradation are considered in more detail in Section 4).

Polymeric materials[8, 20, 33, 44, 50, 58 – 60] [poly(3-hexylthiophene] (P3HT) and its derivatives are most commonly used), low-molecular-weight compounds, in particular pentacene,[24, 35, 61] and oligomers, *e.g.*, α-sexythiophene,[30, 62 – 64] are employed for the fabrication of EGOFETs. The degree of crystallinity of the utilized material[30] and the smoothness of the resulting film[58] are the key factors that influence the stability of semiconductor films, applicable in EGOFETs, in electrolyte solutions. Due to lower mobility of the long polymer chain compared to small molecules, polymeric materials are more suitable for the fabrication of films with high surface uniformity;[65] however, a great advantage of small molecules is that they enable the production of highly crystalline films with high charge mobility.[30]

On the contrary, semiconductor films for OECTs should have a porous structure prone to swelling, and the resulting materials should readily undergo oxidation and reduction.[57, 66] Therefore, the PEDOT : PSS complex is generally employed to fabricate OECTs.[20, 24, 56, 62, 67]

Regioregular poly(3-hexylthiophene) is one of the most commonly applied commercially available semiconductors.[68] Due to the presence of alkyl side chains (Fig. 3 *a*), this compound is readily soluble in most of conventional organic solvents (chloroform, toluene, chlorobenzene, *etc.*). The charge mobility in P3HT-based OFETs fabricated by solution methods reaches 0.2 $cm^2\ V^{-1}\ s^{-1}$.[70] High mobility is due to high crystallinity and ordering of P3HT films, which can self-assemble and form lamellar structures

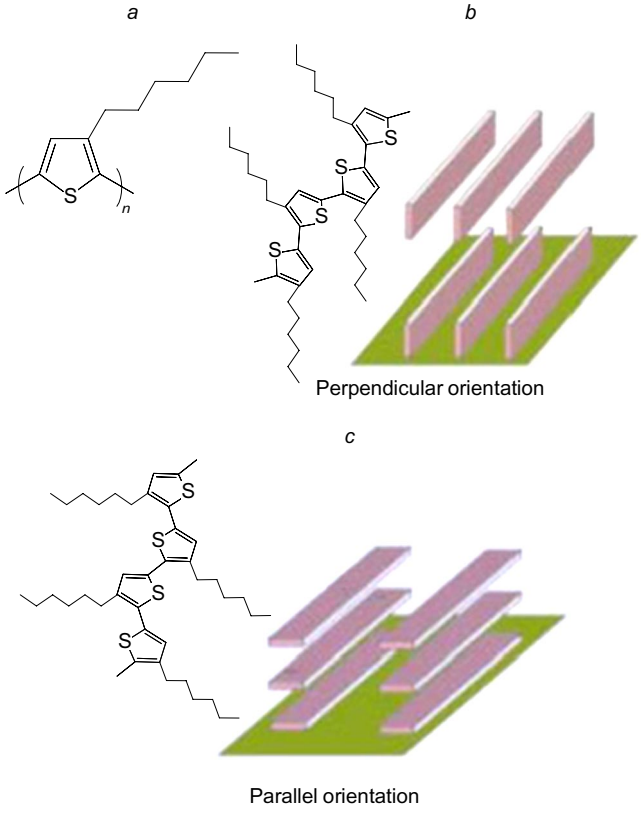
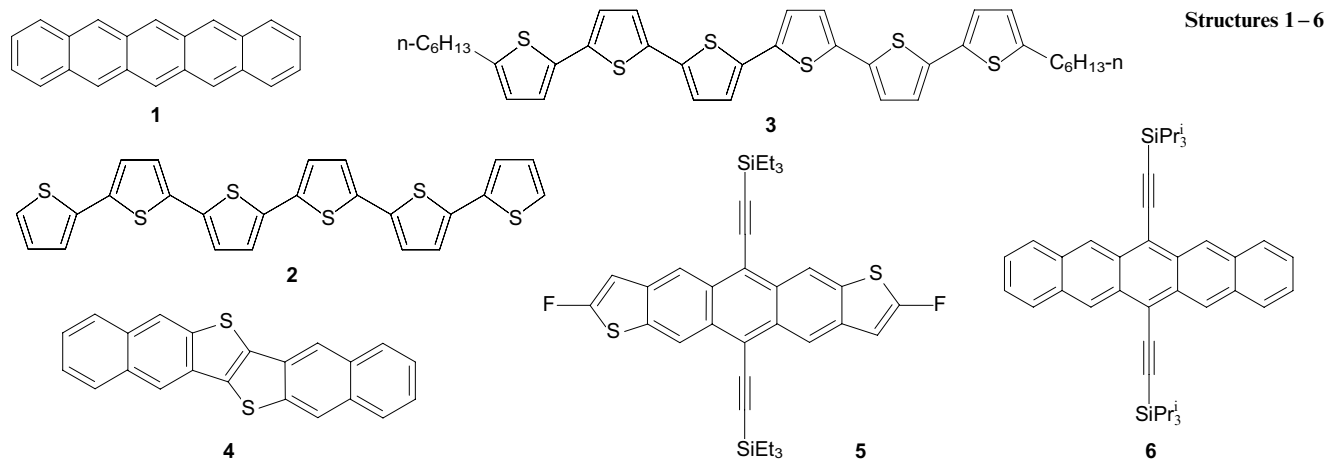



**Figure 3.** Structural formula of P3HT (*a*), perpendicular (*b*) and parallel (*c*) orientations of lamellae in the P3HT film.[69]

**Structures 1 – 6**




1 2 3 4 5 6

(Fig. 3 *b*,*c*). It was shown that the conductivity of P3HT can vary within two orders of magnitude depending on the orientation (parallel or perpendicular with respect to the substrate) of the lamellae; the higher conductivity was found for transistors with a perpendicular lamellar orientation.[30] Besides, high regioregularity and large crystallites of P3HT are required to achieve high charge carrier mobility.[69]

Pentacene is a commonly applied small molecule semiconductor, the molecule of which consists of five fused benzene rings (structure **1**). Since pentacene is poorly soluble, it is usually deposited from the gas phase in high vacuum.[22, 24, 61] The resulting films are characterized by high carrier mobility: higher than 1 $cm^2 V^{-1} s^{-1}$ for OFETs[65] and about $10^{-2}$ $cm^2 V^{-1} s^{-1}$ for EGOTs.[24, 35] Advantages of pentacene are biocompatibility[22] and low cost.[62] The main drawback of pentacene is that it is prone to oxidation in air and when exposed to UV-Vis light.[68] Nevertheless, pentacene-based devices can operate in aqueous solutions over a long period of time due to the dense molecular packing and smoothness of the resulting films.[22, 35]

α-Sexythiophene (α-6T) is an oligomer, the molecule of which consists of six thiophene rings (structure **2**). Generally, α-6T is deposited by thermal evaporation to prepare films that are quite stable in water.[63, 64, 71] The disubstituted analogue of α-6T, α,ω-dihexylsexythiophene (structure **3**), is also utilized in EGOFETs.[72]

The PEDOT : PSS polyelectrolyte complex is synthesized by the oxidative polymerization of the 3,4-ethylenedioxythiophene (EDOT) monomer in the presence of an excess of the negatively charged polyelectrolyte polystyrene sulfonic acid (PSS), which stabilizes negatively charged PEDOT chains produced in the synthesis to form a water-stable dispersion. This dispersion consists of PEDOT : PSS polyelectrolyte complex gel particles in water. This gel is stable in acidic environment due to the presence of excess PSS. The drying of PEDOT : PSS gel particles affords a homogeneous transparent conducting film. The changes in the size of such particles and in the ratio of PEDOT and PSS in the course of the synthesis, changes in the composition of the solvent during drying and the use of particular conditions of fabrication significantly affect the morphology of the conducting film, thereby making it possible to vary the conductivity within many orders of magnitude (from $10^{-5}$ to $10^3$ S $cm^{-1}$).[73] Due to these characteristics, PEDOT : PSS is widely employed as a conducting material for the fabrication of electrodes and as a material for semiconductor layers. The ion permeability of PEDOT : PSS films in aqueous solutions is due to their porous and hydrophilic structure (Fig. 4).[20] High conductivity typical of PEDOT : PSS films is observed when small domains of PEDOT nanofibrills (blue strips in Fig. 4) are surrounded by PSS polymer chains. The self-assembly of PEDOT giving small domains is facilitated by the slow solvent drying after the film deposition, which is provided by the addition of the high-boiling polar solvent DMSO to an aqueous solution of PEDOT : PSS.[20, 74]

The above-considered organic semiconductors are most often used for the fabrication of EGOTs. However, the range of semiconductors applied for the creation of EGOTs is not limited to these compounds. Worthy of notice are such small molecules as dinaphtho[2,3-*b*:20,30-*f*]thieno[3,2-*b*]thiophene[53, 75] (structure **4**), 2,8-difluoro-5,11-bis(triethylsilylethynyl)anthradithiophene[23, 36] (structure **5**) and 6,13-bis(triisopropylsilylethynyl)pentacene[36] (structure **6**). Poly[2,5-bis(3-tetradecylthiophen-2-yl)thieno[3,2-*b*]thiophene] (structure **7**) was utilized as a polymeric material.[59] Lenz *et al.*[25] employed the diketopyrrolopyrrole – terthiophene donor – acceptor copolymer (structure **8**).

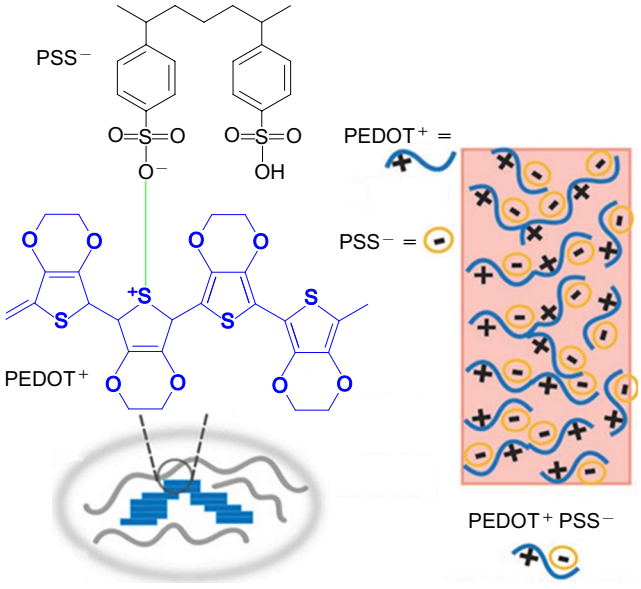
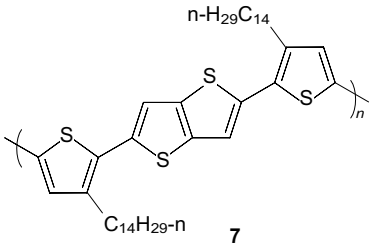
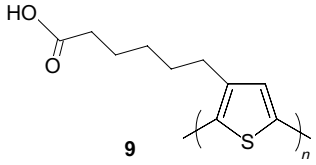



**Figure 4.** Structure of the ion-permeable PEDOT : PSS layer.[20, 74]

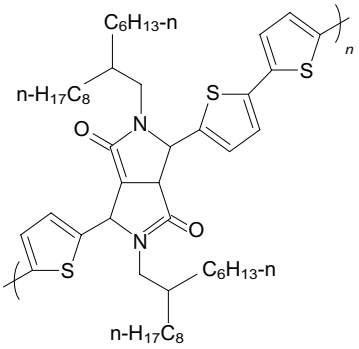
**Structures 7 – 10**



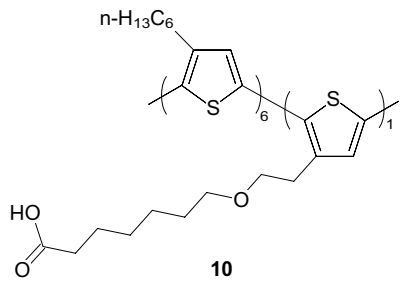

**7**




**9**




**8**




**10**

For a long time, the development of semiconductor materials for EGOTs was based mainly on the modification of commercially available materials,[65] such as P3HT. In addition to the preparation of a film stable in electrolytes, the fabrication of biosensors requires the introduction of functional groups allowing the attachment of the biorecognition layer to the semiconductor surface.[76–78] In the case of solid electrolytes, the semiconductor surface should be hydrophilized to facilitate the deposition of the electrolyte layer.[39,47]

For instance, Toss *et al.*[76] described two P3HT derivatives as semiconductor materials for EGOTs — poly-3-carboxypentylthiophene (P3CPT) (structure **9**) and the P3HT – co – poly(3-ethoxypentanoic acid thiophene) copolymer (P3HT-COOH15) with a monomer ratio of 1 : 6 (structure **10**). The authors introduced carboxy groups as possible anchoring sites for biorecognition elements. It was shown that more hydrophobic P3HT-COOH15, like the initial P3HT, operates in the EGOFET mode, while the electrochemical operation mode was suggested for P3CPT at voltages above −0.8 V. Magliulo *et al.*[77] also functionalized the P3HT surface with carboxy groups using the plasma-enhanced chemical vapour deposition technique. Sinno *et al.*[78] employed the P3HT – co – poly(*N*,*N*-dimetylaminoethyl methacrylate) polymer for the hydrophilization.

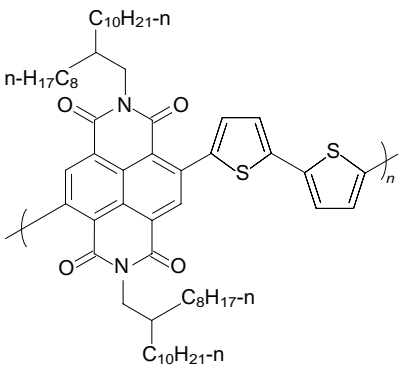
In recent years, the progress in organic bioelectronics resulted in a growing number of publications devoted to semiconductor materials for EGOT. Significant advances made in this field are considered by Borges-González *et al.*[65] in the review on organic semiconductors for biosensors. Apart from p-type semiconductors, there have been an increasing number of new organic n-type semiconductors developed for the application in EGOTs as elements for low-voltage computing systems, which require both p- and n-type transistors.[39,65,66,79,80]

Porrazzo *et al.*[79] demonstrated the possibility of using some known electron-transporting polymer semiconductors (structures **11** – **13**) in EGOTs and also reported the application of the fabricated devices, which were integrated with conventional p-type EGOTs to obtain inverting logic gates. Pure water was used as the electrolyte in direct contact with the semiconductor layer. Devices based on phenyl-$C_{61}$ butyric acid methyl ester (structure **13**) exhibited the best performance at the initial moment; however, a marked threshold voltage shift towards lower voltages was recorded after 3 min in continuous contact with water.

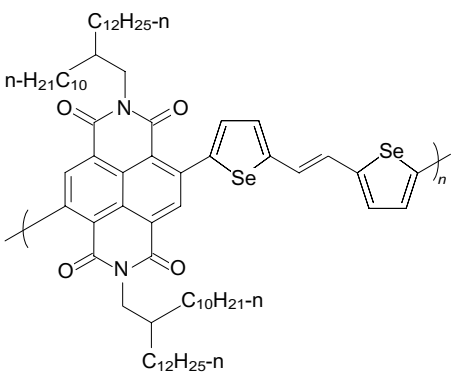
Giovannitti *et al.*[66] synthesized a semiconductor polymer material and used it to develop an ambipolar OECT. The device supported both electron and hole transport and retained performance characteristics when tested for 2 h under continuous cycling in water. The material was synthesized in two modifications, which differ by side groups (Scheme 1). Both polymers have a narrow band gap (1.68 and 0.71 eV) and, consequently, were easily doped with an aqueous electrolyte or atmospheric oxygen. In the measurements in a NaCl aqueous solution, the injection of $Na^+$ or $Cl^-$ ions was observed depending on the charge of the doped semiconductor. Therefore, the results of this study open the possibility to develop complementary circuits based on OECTs and provide a way to improve the sophistication of bioelectronic devices.

Sun *et al.*[80] demonstrated that n-type OECTs based on ladder-type conducting polymers can exhibit high transconductance (up to 9.7 mS) in aqueous solutions (see Fig. 5). These data were obtained using poly(benzimidazobenzophenanthroline) (structure **14**) as the semiconductor.

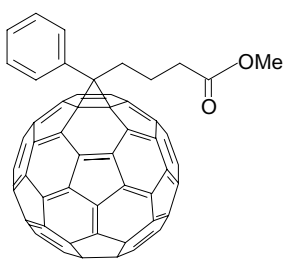
**Structures 11 – 13**




**11**

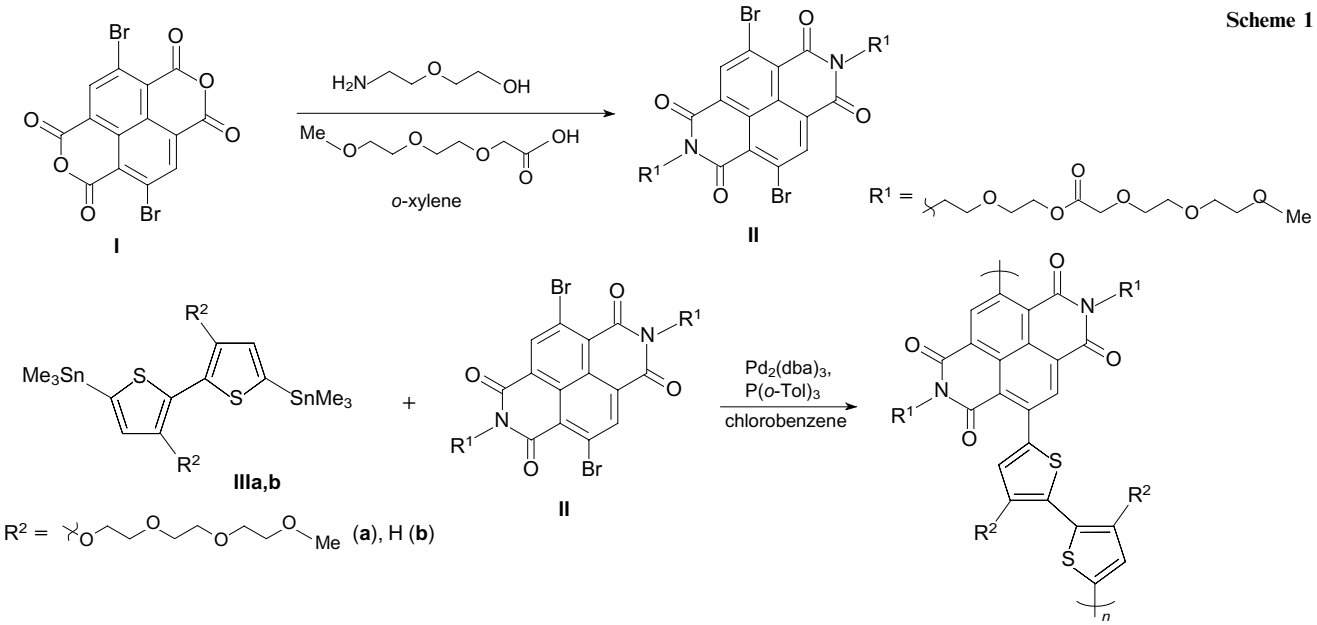



**12**

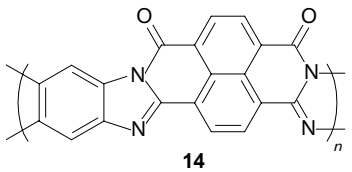



**13**

**Scheme 1**




**Structure 14**



**14**

The device showed high stability in water during pulse measurements over one hour.

Nielsen *et al.*[57] reported the molecular design of semiconductor polymers for OECTs. The authors prepared five new polymers based on different thiophene derivatives entailing triethylene glycols (TEGs) as side chains (structures **15** – **19**). The relationship between the chemical structure and properties of the synthesized materials was analyzed in detail. The authors also revealed key elements of the molecular architecture, which allow the enhancement of the hole and ion transport. The hole transport was facilitated by the thiophene-containing polymer backbone and the ion transport was facilitated by the TEG side chains of the polymer. Polymers based on TEG derivatives of bithiophene were shown to be electrochemically more stable than polymers based on TEG derivatives of benzodithiophene. The low density of TEGs (polymer **18**) proved to be more favourable for the efficient π-conjugation of the side chains than the high density (polymer **19**). Organic electrochemical transistors based on polymer **18** showed higher charge mobilities for the hole transport (0.28 $cm^2 V^{-1} s^{-1}$) compared to those based on polymer **19** (0.01 $cm^2 V^{-1} s^{-1}$). This fact was attributed to higher flexibility of the backbone facilitating the creation of more efficient π-conjugation and better film morphology. Devices

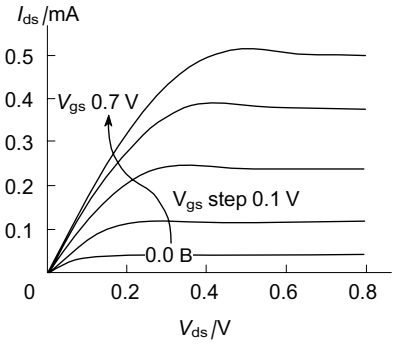
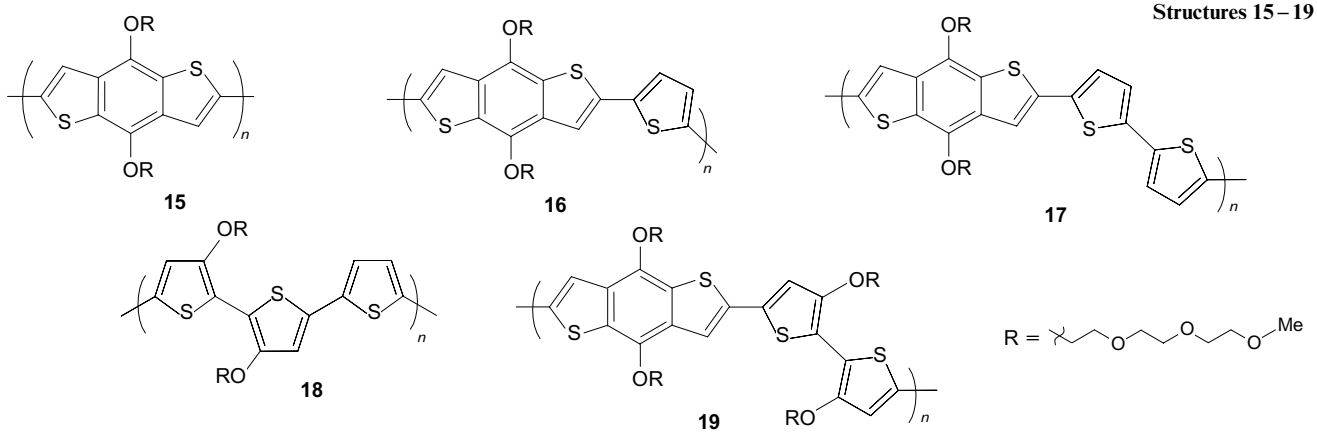



**Figure 5.** Transfer characteristics of OECT based on poly(benzimidazobenzophenanthroline) **14**.[80]

**Structures 15 – 19**



based on compound **18** exhibited peak transconductance of $>20$ mS, $I_{ds}$ values of several mulliampers and $I_{on/off} > 10^5$. These devices have better performance compared to analogues based on PEDOT : PSS and showed stability under operation in water medium without the need for additives or cross-linking agents.

Therefore, the design of new semiconductor materials and chemical modification of commercial semiconductor materials make it possible to significantly extend the range of application of EGOFETs and OECTs due to the improvement of their electrical characteristics, enhancement of stability and performance reproducibility and an increase in the operational lifetime and also open new possibilities to use EGOTs as elements for low-voltage computing.

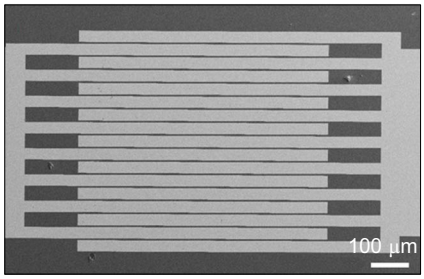



**Figure 6.** Scanning electron microscope (SEM) image of interdigitated contacts coated with the P3HT film.[85]

### 3.2. Materials for electrodes and substrates

Gold is most commonly used for the fabrication of drain and source contacts due to its high electrochemical stability, excellent electrical conductivity and low contact resistance when employed in combination with p-type semiconductors.[19] To improve the mechanical adhesion between the electrodes and the substrate, a thinner chromium [23, 81] or titanium [53] adhesion layer is often plated under the gold layer. However, gold is an expensive material with a high work function (5.3 eV). Hence, gold electrodes are not suitable for electron-transporting EGOTs and for the fabrication of disposable devices. Conducting polymers, generally highly conducting PEDOT : PSS, are employed as an alternative to gold.[62, 82] Conducting polymers can be deposited by printing techniques, thereby significantly reducing the cost of device fabrication. However, the conductivity of such polymers is rather lower compared to metals. The possibility of using indium tin oxide, oxidized graphene and silver nanoparticles as materials for contacts in EGOTs was considered by Hong *et al.*[19] These materials have a conductivity comparable to that of gold and can be deposited by printing techniques.

Platinum is usually employed as a gate electrode material.[23, 51] Nevertheless, other materials were also used for the fabrication of gate electrodes. For example, gold was utilized in some experiments [9, 26] because it can more easily be modified with organic molecules for the creation of biosensing layers. Horowitz and co-workers [29] investigated the application of different materials for gate electrodes, including gold, platinum, tungsten, copper, silver and glassy carbon. It was shown that the threshold voltage of the device depends on the work function of the gate material. Thus, the threshold voltage for tungsten with a work function of 4.65 eV was $-0.31$ V, while the threshold voltage for platinum with a work function of 5.65 eV was $-0.09$ V (for EGOT with hole mobility). In some cases, electrodes are modified with self-assembled interfacial layers [84] in order to change the work function [83] or improve the morphology of the semiconductor layer.[36] This modification, like the use of polymer electrodes, provides biocompatibility of the end device.

Electrolyte-gated organic transistors are fabricated using mainly interdigitated drain – source contacts (Fig. 6), because interdigitated circuits allow a significant increase in the channel width ($W$) at a fixed channel length ($L$). According to Eqn (8), $I_{ds}$ is proportional to the $W/L$ ratio. Hence, interdigitated circuits make it possible to increase the current in the transistor cannel and reduce the relative error of measurement. The interdigitated electrodes are more frequently utilized in EGOTs than in OFETs, because the $I_{ds}$ values measured based on an EGOT platform are generally significantly smaller than those based on OFET. This is primarily due to the fact that the charges in EGOTs move in the inhomogeneous upper part of the semiconductor film,[29] while charges in OFETs move in the lower layer near the semiconductor/dielectric interface.[86] The interdigitated contacts enable a significant increase in $I_{ds}$, while the leakage current $I_{gs}$ remains unchanged.

A substrate for EGOTs serves as a platform, which is coated with a semiconductor and contacts. Hence, materials for the substrates should be stable, non-conducting and have a smooth surface. Highly doped silicon wafers coated with thermally oxidized silicon dioxide as the dielectric layer are most commonly employed for this purpose. Such wafers allow the use of the devices both in the EGOT mode with the top gate immersed in the electrolyte and in the OFET mode with conducting layer of doped silicon as the bottom gate electrode.[25, 52, 87] Such devices permit the measurement of, *e.g.*, the EDL layer capacitance in the electrolyte.[35] Quartz is also widely utilized in EGOT substrates.[9, 51] Di Lauro *et al.*[61] demonstrated that the quartz substrate can be considered as the pH-controlled second gate. Such polymer materials, as polyethylene terephthalate (trade name Mylar) [38, 88, 89] polyethylene naphthalate [90] and polyimide (Kapton) [23] also widely serve as substrates. Polymer materials can be used to fabricate flexible biocomaptible [23, 90] devices solely by printing techniques to reduce their cost.

Therefore, the performance of EGOTs can be improved and the device fabrication cost can be reduced by selecting appropriate materials for substrates and electrodes. Selected materials can be made biocompatible *via* modification (see below).

## 4. Operation stability of electrolyte-gated organic transistors

The main drawback of EGOFETs and OECTs, which limits their potential use in practice, is electrical worsening during operation.[36] The long-term operations of electrolyte-gated transistors lead to a decrease in the maximum source-to-drain current and the threshold voltage shift.[1, 79, 85] Threshold voltage shifts are often already observed in the second measurement, which is manifested as the hysteresis in $I-V$ curves. The main factors that adversely affect the electrical characteristics of electrolyte-gated transistors are the appearance of new defects on the surface and in the bulk of the organic semiconductor, charge carrier injection from the electrolyte layer to the semiconductor (unwanted in the case of EGOFETs), possible electrochemical reactions

between the electrolyte, contacts and the semiconductor layer [91, 92] and the oxidation of the semiconductor with atmospheric oxygen.

Since the operation stability is a critical parameter for all transistors, particularly for those used as sensing elements, testing methods were developed for the evaluation of stability of EGOTs. There are three most commonly used methods, which are applied for testing OFETs as well.[36, 93 – 95] According to one procedure, the time dependence of the electrical current is measured during continuous operation of an electrolyte-gated transistor. For this purpose, constant voltages are applied to the source, drain and gate of the device. Another procedure is based on cyclic measurements of $I-V$ curves of an electrolyte-gated transistor. The transistor is switched on for a short period of time at a constant voltage, then $I-V$ curves are measured and the cycles are repeated until a significant decrease in the characteristics of the transistor is observed. According to the third method, the operation stability of an electrolyte-gated transistor is tested over a long period of time (for several weeks) under shelf-life conditions, one measurement of $I-V$ curves being conducted once a day. In intervals between the measurements, the device is washed, dried and stored under ambient conditions.

Picca *et al.*[85] evaluated the operation stability of EGOFET based on P3HT deposited by spin-coating solution in chlorobenzene. Previously, it was demonstrated that the use of chlorobenzene as the solvent leads to the formation of crystalline P3HT films with high carrier mobility.[96] The surface of P3HT films was studied by atomic force microscopy (AFM) and X-ray photoelectron spectroscopy (XPS). The measurements conducted at certain intervals demonstrated that, after operating in water for two weeks, the surface roughness of the film increased; however, no deep defects or cracks were observed (Fig. 7). According to the XPS data, the oxygen content of the film increased from $9.1 \pm 0.2$ at.% to $\sim 10.4 \pm 0.2$ at.%.

Picca *et al.*[85] developed a protocol for measuring the transfer characteristics of EGOFETs based on the application of pulse voltages. The results of measurements of transfer characteristics and of the leakage current as a function of the voltage in the direct current and pulse modes are presented in Fig. 8 *a*,*b*. It is seen in Fig. 8 that the leakage current measured in the pulse mode reaches much lower values than those in the direct current mode,

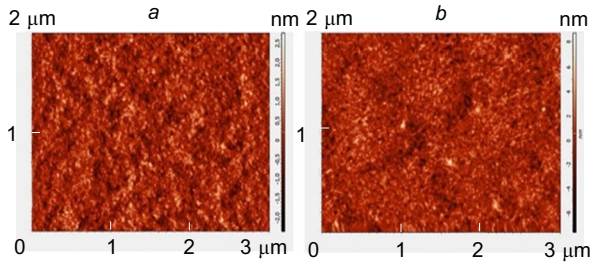



**Figure 7.** Atomic force microscopy (AFM) images of the P3HT surface before (*a*) and after (*b*) two weeks under water.[85]

*i.e.*, the application of the pulse mode is promising for maintaining the operation stability of the device. Figure 8 *c* displays the results of measurements of the maximum current $I_{ds}$ under continuous operation of the device for 7 days; the inset in this figure shows the observed threshold voltage shift. These results are adequately approximated by a double exponential decay function with time constants equal to $1.8 \pm 0.5$ and $35 \pm 3$ h (red curve in Fig. 8 *c*). The presence of two exponents is indicative of fast and slow polymer degradation processes, the fast process being reversible, while the slow one being irreversible. The slow process was attributed [85] to the charge trapping in the semiconductor. The shelf-life time test demonstrated that the maximum operating life of the devices is $\sim 20$ days. In order to increase this time frame, 1% agarose gel was applied to the polymer semiconductor surface after each measurement and then washed before use. In intervals between the measurements, the device was stored in the dark. This strategy made it possible to extend the service life of the device by more than 60 days due apparently to the barrier properties of the gel, which protects the semiconductor from oxidation by atmospheric oxygen.

Nguy *et al.*[58] evaluated the operation stability of P3HT-based EGOFET deposited on the silicon substrate by spin coating. The threshold voltage $V_t$ and the current ratio $I_{on/off}$ were measured as a function of the surface roughness of the semiconductor (Fig. 9 *a*). The threshold voltage was almost independent of the surface roughness and was about $-0.4$ V in all cases. Meanwhile, the surface roughness had a significant effect on $I_{on/off}$ and its reproducibility. Thus, for the film with a roughness of 0.5 nm, the ratio $I_{on/off}$ was

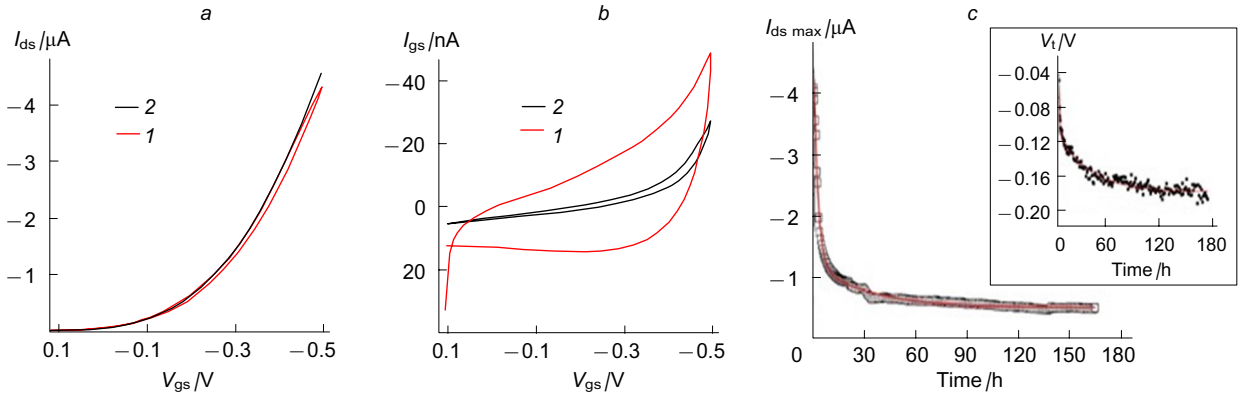



**Figure 8.** Dependences of the drain – source current (*a*) and the gate – source current (leakage current) (*b*) on the voltage at the gate measured in the continuous (*1*) and pulse (*2*) modes; (*c*) the maximum drain – source current (the threshold voltage shift in the inset) as a function of the sensor operation time.[85]

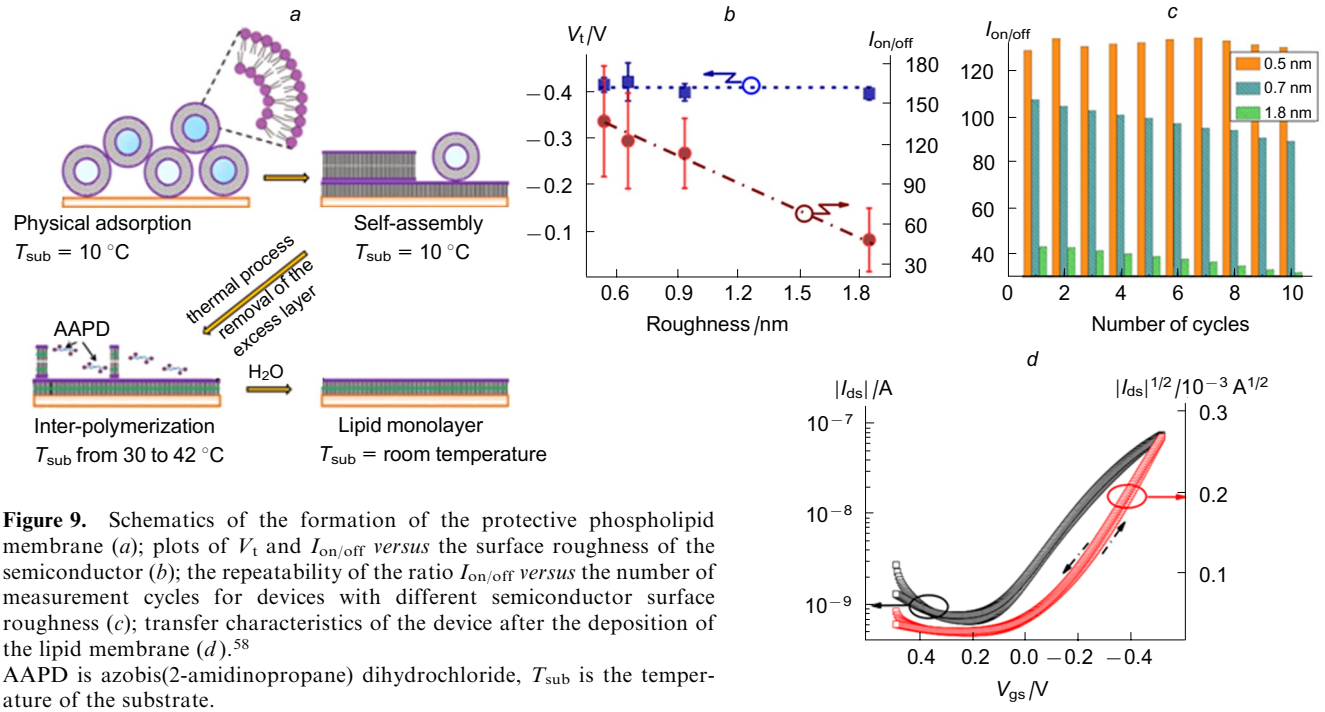



**Figure 9.** Schematics of the formation of the protective phospholipid membrane (*a*); plots of $V_t$ and $I_{on/off}$ *versus* the surface roughness of the semiconductor (*b*); the repeatability of the ratio $I_{on/off}$ *versus* the number of measurement cycles for devices with different semiconductor surface roughness (*c*); transfer characteristics of the device after the deposition of the lipid membrane (*d*).[58]
AAPD is azobis(2-amidinopropane) dihydrochloride, $T_{sub}$ is the temperature of the substrate.

~135, while $I_{on/off}$ decreased by a factor of three for the film with a roughness of 1.8 nm. The films with the lowest roughness demonstrated the best stability and $I_{on/off}$ repeatability (see Fig. 9 *b*).

Nguy *et al.*[58] tested the hypothesis that the operation stability of EGOFETs can be improved by the deposition of 1,2-bis(10,12-tricosadiynoyl)-*sn*-glycero-3-phosphocholine as the protective phospholipid layer on the semiconductor surface. The layer was formed from a solution of unilamellar phospholipid vesicles, which underwent degradation upon physical adsorption, being self-assembled to an extended multilayer. Upon subsequent heating to 30 °C, the outer phospholipid layers were dissolved, resulting in the formation of a monolayer membrane with a thickness of ~2 nm (see Fig. 9 *c*). The mechanical stability of the resulting membrane was provided *via* inter-polymerization involving acetylene groups in the presence of azobis(2-amidinopropane) dihydrochloride as the radical initiator. The formation of the phospholipid membrane on the EGOFET surface was confirmed by Fourier-transform spectroscopy and by the change in the wetting contact angle of the device. The modification with the phospholipid layer led to a decrease in the current $I_{ds}$ by almost an order of magnitude compared to $I_{ds}$ for the unmodified EGOFET, the threshold voltage shift towards +35 mV and the disappearance of the hysteresis (see Fig. 9 *d*). Therefore, the phospholipid membrane improved the operation stability of the device; however, it somewhat impaired its $I-V$ curve. Apparently, an increase in the operation stability of the EGOFET was attributed to the fact that the membrane prevented water adsorption by the semiconductor and reduced the charge carrier trapping in the semiconductor from the solution.

Lee *et al.*[97] examined the factors responsible for irreversible degradation of polyaniline nanowire-based EGOFETs. The nanowire was placed on the surface of two gold

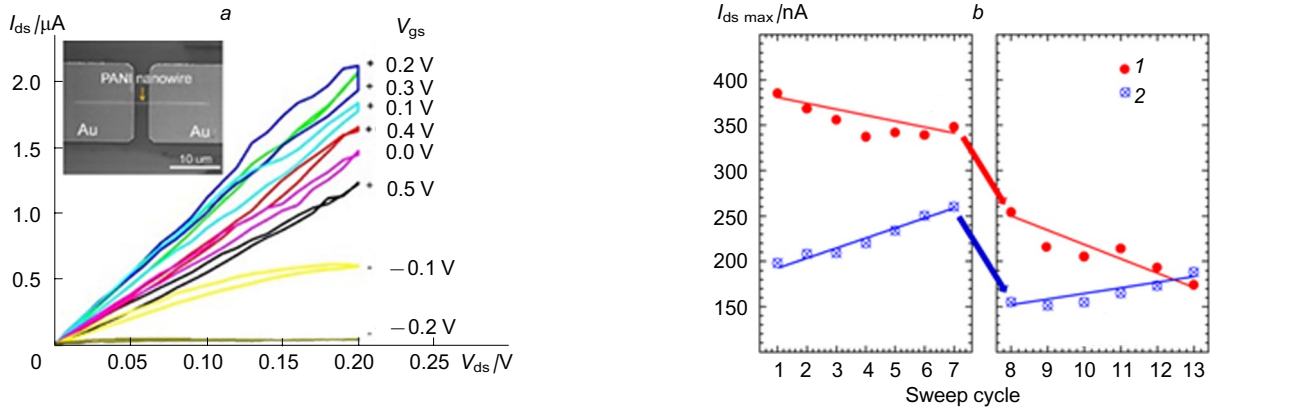


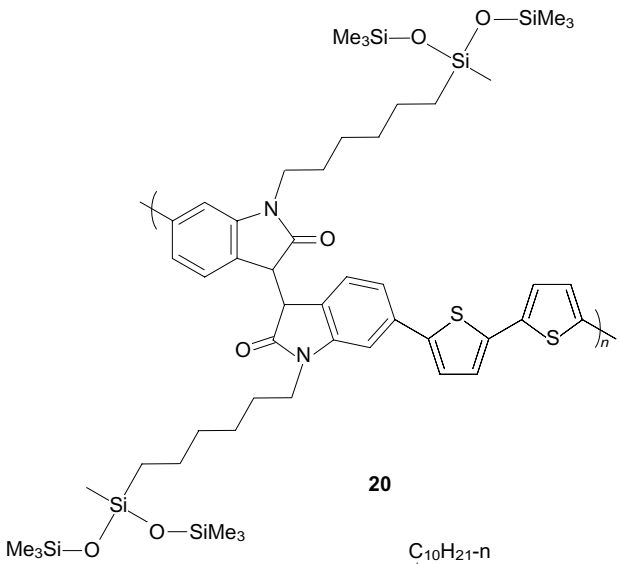

**Figure 10.** Output characteristics of polyaniline nanowire-based EGOFET; the inset shows the SEM image of EGOFET (*a*); cyclic measurements of the maximum drain – source current in EGOFET at $V_{ds}$ = 0.1 V (*b*).[97]
(*1*) Positive sweep (oxidation); (*2*) negative sweep (reduction).

contacts. The SEM image of the fabricated EGOFET is shown in the inset in Fig. 10 *a*. An analysis of a series of output $I-V$ curves (Fig. 10 *a*) shows that the conductivity increases with increasing $V_{gs}$ from $-0.2$ to $+0.2$ V and then again decreases with increasing $V_{gs}$ from $+0.3$ to 0.5 V, which is in agreement with the data obtained in the previous experiments.[92] These behaviour was attributed to the irreversible oxidation of the nanowire at high voltages. For a series of transfer $I-V$ curves, the maximum values of $I_{ds}$ decreased during the positive sweep corresponding to the oxidation, whereas these values, on the contrary, increased during the negative sweep with increasing number of sweep cycles up to 13 (Fig. 10 *b*). These observations were accounted for by a gradual decrease in the contribution of Coulombic repulsion due to the trapped charges in the new electronic level. It should be noted that a significant decrease in the conductivity after seven cycles is associated with the refilling of the electrolyte solution, during which the nanowire was exposed to atmospheric oxygen, resulting in the partial blocking of conducting pathways by adsorbed oxygen.

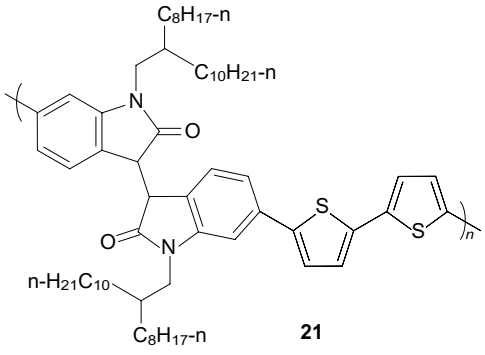
Knopfmacher *et al.*[50] described EGOFETs based on a series of polyisoindigo-containing polymers (structures **21** – **23**). Heptamethyltrisiloxane substituents were introduced into polymer **20** in order to increase its solubility. The main advantage of these materials is their stable long-term performance in deionized water and seawater. The semiconductor layer was deposited by spin coating followed by annealing. The authors stated that the annealing led to a decrease in the fraction of non-operating devices to 17% of their total number. The fabricated device was used as a chemical sensor capable of detecting heavy metal cations, in particular $Hg^{2+}$, in water in the presence of other ions. Most of the sensing measurements were implemented on the OFET platform using the bottom-contact gate electrode of the device (see Fig. 11 *a*) at $V_{ds}$ of up to $-1$ V and $V_{gs}$ of up to $-5$ V. The performance of the device remained stable for 17 days, although the measurements showed an increase in the hysteresis of $I-V$ curves compared to the measurements performed in the absence of water, which was attributed to the diffusion of ions from the solution inside the bulk of the semiconductor through cracks in the film and the appearances of charge carrier traps. The EGOFET-based measurements were conducted at $V_{ds}$ of up to $-1$ V and $V_{gs}$ of up to $-0.6$ V (see Fig. 11 *b*).

In order to explain high stability of polymer **20** in aqueous solutions, this polymer was compared with reference semiconducting polymer **21**, which has the same backbone but contains branched alkyl side chains instead of siloxane groups. Reference polymer **21** significantly degraded when operating in water over two days. Knopfmacher *et al.*[50] attributed this fact to the less dense packing of the polymer containing alkyl side chains compared to its siloxane analogues. In the case of polymer **20**, the observed stability of measurements was accounted for by the presence of siloxane groups and a short intermolecular $\pi-\pi$ stacking distance (3.58 Å), whereas this distance in reference polymer **21** is 3.76 Å. Polymers **22** and **23**, which are stable in air and have energy level systems similar to those in polymers **20** and **21**, were investigated in order to demonstrate the important role of intermolecular $\pi-\pi$ stacking distances in semiconductors. This distance in polymers **22** and **23** is $< 3.6$ Å. The investigations demonstrated that EGOFETs based on these polymers have good stability in water. In Supplementary materials, the authors noted that there is a

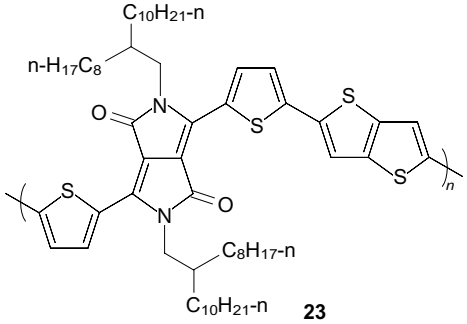
**Structures 20 – 23**



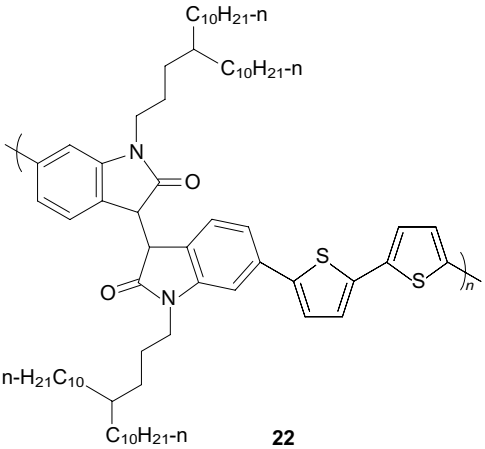

**20**




**21**




**23**




**22**

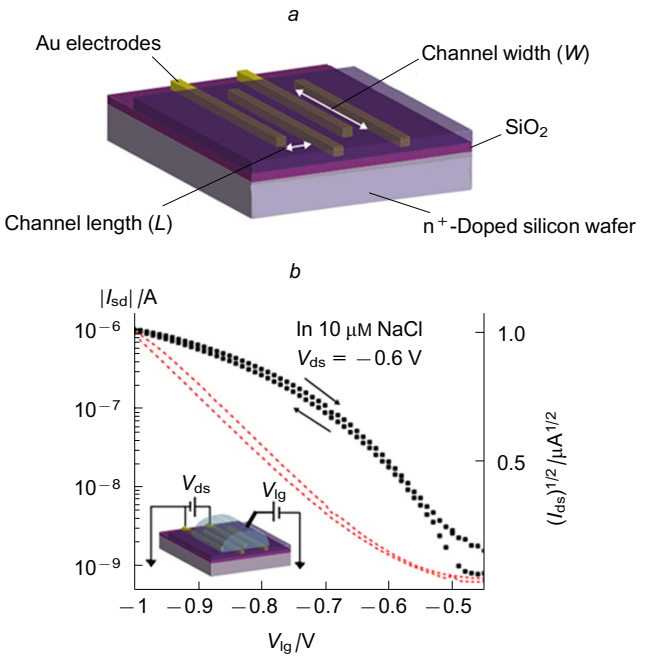



**Figure 11.** Schematic of the fabricated electrolyte-gated device (*a*) and its output characteristics (*b*); the inset shows the schematic of the measurement set-up based on EGOFET.[50]
In the measurements using the electrolyte gate, $V_{gs}$ was denoted as $V_{lg}$ (liquid gate).

certain threshold value for the layer thickness of polymers with a short π–π stacking distance. Thus, thicker polymer layers with a short π–π stacking distance (in the polymers under consideration, this value is ~30 nm) were stable in aqueous media. However, the nature of this phenomenon was not discussed and it is an interesting issue for further research.

Therefore, the degradation of EGOFETs during their storage and operation can be caused by a number of factors, in particular, the applied voltage, impairment of morphology of the semiconductor layer (an increase in the film roughness) in contact with the electrolyte, the initially insufficiently dense packing of semiconductor molecules in the layer and the irreversible oxidation of the semiconductor. These factors pose serious problems for the practical application of EGOFET-based devices. Possible ways of increasing the service life of these devices include the application of protecting materials during their storage and operation, the sparing mode of measurements (pulse voltage application) and the design of new semiconductor materials having high thermooxidative stability and ability to crystallize in thin films.

## 5. Application of electrolyte-gated organic transistors

### 5.1. Biosensors

According to the IUPAC definition, a device that uses specific biochemical reactions mediated by isolated enzymes, immunosystems, tissues, organelles or whole cells to detect chemical compounds usually by electrical, thermal or optical signals..[98] The application of EGOTs as biological liquid sensors has attracted great attention.[1,3,9–11,23,99,100] This is primarily due to the fact that these devices operate at low voltages, which do not cause degradation of biomolecules. Besides, organic materials are often biocompatible and, consequently, they can be employed to fabricate sensors for the on-line monitoring of health conditions of patients.[101–103]

The fabrication of EGOFET-based biosensors involves the modification of the gate surface (Fig. 12 *a*) or the semiconductor surface (Fig. 12 *b*) with molecules capable of specifically binding to analyte molecules.

Semiconductors are functionalized *via* the formation of covalent bonds with molecules of the biorecognition layer or through physical adsorption of the biorecognition layer on the semiconductor.[10,30] The methods of immobilization of enzymes, antibodies, aptamers and other molecules on the semiconductor or gate surface are considered in more detail by Wang and co-workers.[104]

Changes in the electrical parameters of biosensing systems serve as an analytical signal in EGOT-based biosensors. These parameters include the threshold voltage,[10,36] the drain–source current (the quantitative parameter is the current change with increasing concentration divided to the current in the absence of the analyte in the solution), the charge mobility and the transconductance.[9–11,29,59] Seshadri *et al.*[10] suggested that the observed changes in the electrical parameters may be, in particular, attributed to the interaction between the receptor and the analyte, which causes a conformational change of the receptor molecule and, consequently, a change in the morphology of the modified surface. Since the thickness of the dense part of EDL is a few angströms,[44] the change in the morphology influences the charge transport in the conducting channel, which can be observed from the change in the slope of the linear region of transfer curves. The analyte can cause a change in the charge distribution over the biologically modified surface: the analyte can serve as a charge trapper

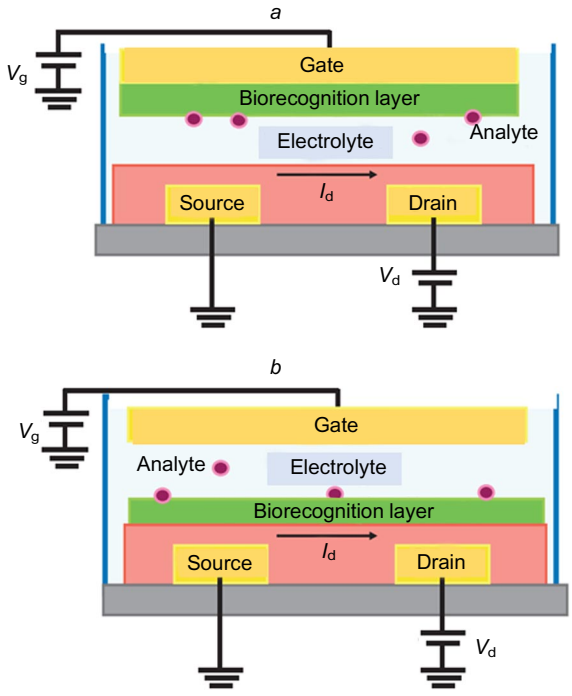



**Figure 12.** Architecture of the EGOT-based biosensor. The biorecognition layer is attached to the gate electrode surface (*a*) or the semiconductor surface (*b*).[20]

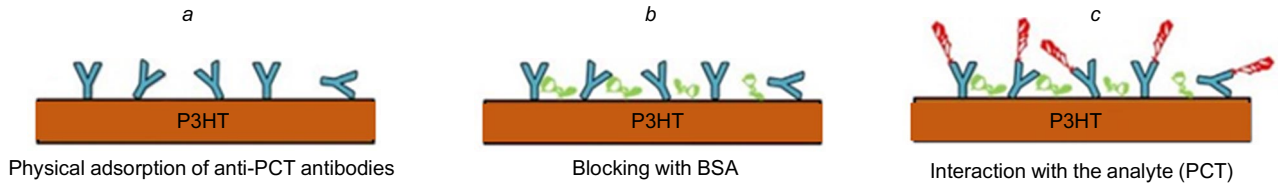



**Figure 13.** Schematics of the P3HT semiconductor channel with immobilized layers of monoclonal antibodies (*a*), bovine serum albumin (*b*) and the receptor layer after the interaction with PCT (*c*).[10]

or, on the contrary, as a source of additional charges in the semiconductor layer.[10] This affects the charge mobility or the threshold voltage shift. The additional contribution to the total capacitance of the system upon the addition of the receptor layer is yet another important factor.[20]

Torsi and co-workers [10] developed an immunosensor for the detection of procalcitonin (PCT), known as a good marker of sepsis, in solution. In this sensor, P3HT deposited by spin coating served as the organic semiconductor. After the annealing, monoclonal antibodies specific to PCT were immobilized on the P3HT surface by the deposition from the solution (Fig. 13).

To increases the specificity of antibodies to PCT, the immobilization of antibodies on the semiconductor surface (Fig. 13 *a*) was followed by the post-treatment with bovine serum albumin (BSA) as the blocking agent. Figure 14 presents the changes in the relative threshold voltage and charge mobility as a function of the PCT concentration in the solution. The selectivity of the antibody-immobilized sensor to a PCT solution was demonstrated in assays in dissolved milk powders. The immunosensor was used to detect PCT in the concentration range from $10^{-12}$ to $10^{-8}$ mol $L^{-1}$. The detection limit of the immunosensor was ~2.2 pmol $L^{-1}$, which is within a range of clinical relevance: the PCT concentration in the blood of healthy individuals is not higher than 4 pmol $L^{-1}$, and it increases

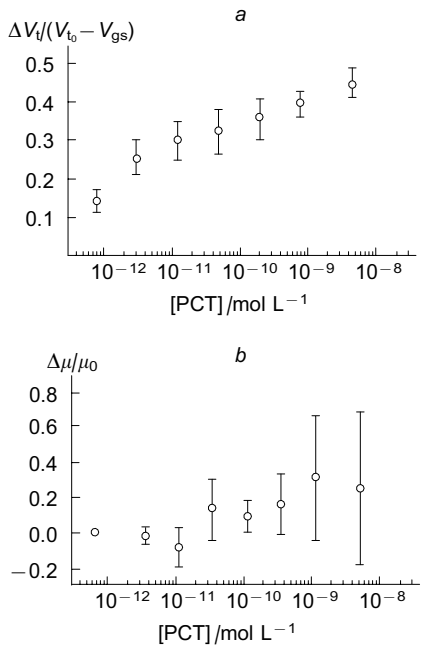



**Figure 14.** Relative changes in the threshold voltage $[\Delta V_t/(V_{t0} - V_{gs})]$ (*a*) and the charge mobility ($\Delta\mu/\mu_0$) (*b*) as a function of the PCT concentration.[10]

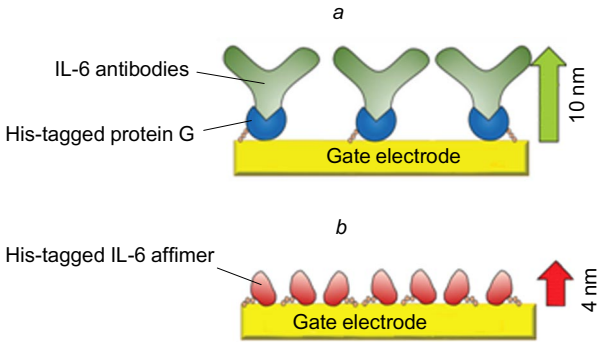



**Figure 15.** Schematics of the gold gate functionalized by two methods: IL-6 antibodies were immobilized on the gate surface through histidine (His)-tagged protein G (*a*) and anti-IL-6 affimers were immobilized directly on the gold surface through His-tag (*b*).[13]

by more than three orders of magnitude in patients with sepsis.

Biscarini's research group [13] developed an EGOFET-based immunosensor and an aptasensor for the detection of interleukin-6 (IL-6), a multifunctional cytokine, which has context-dependent pro- and anti-inflammatory properties.[105] High IL-6 levels are known to be associated with some chronic inflammatory pathologies and cancer. Two EGOT-based sensors with the functionalized gate were developed: with immobilized monoclonal antibodies (Fig. 15 *a*) and with peptide aptamers (affimers) (Fig. 15 *b*).

The gate was functionalized according to a procedure described by Biscarini and co-workers.[16,99] Pentacene was used as the semiconductor material. Ten pentacene monolayers (with a total thickness of 15 nm) were deposited on the substrate by thermal vacuum sublimation. Figure 16 presents the sensing response as a function of the IL-6 concentration for the antibody-based device. The following value served as a response for both the antibody-based sensor and the aptamer-based sensor:

$$S = -\frac{I_n - I_0}{I_0} \qquad (19)$$

where $I_n$ is the drain – source current at the $n$th concentration of IL-6 and $I_0$ is the current at the zero concentration of IL-6. The detection limit of IL-6 was about 1 pmol $L^{-1}$ for both types of devices, which is lower than the IL-6 level in the human serum of patients with inflammatory response.

Berto *et al.*[11] developed a new EGOFET-based immunosensor for the detection of the extracellular protein anti-inflammatory cytokine tumour necrosis factor (TNF). Peptide aptamers were used as bioreceptors instead of traditional antibodies; pentacene served as the semiconductor. Aptamer-based sensors (aptasensors) demonstrated high

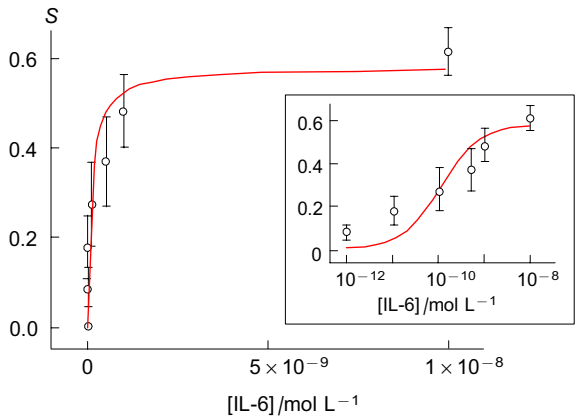



**Figure 16.** Sensing response ($S$) as a function of the IL-6 concentration for the device based on His-tagged protein G. The inset shows the sensing response as a function of the logarithm of the IL-6 concentration for the same device.[13]

sensitivity and good stability. The functionalization of the gate electrode surface involved the attachment of histidine-tagged recombinant protein G to the electrode surface followed by the immobilization of antibodies against TNF *via* binding to the protein G. The gate regions that remained uncoated were passivated by soaking in a BSA solution.

The AFM images of the gold contact surface presented in Fig. 17 *a*,*b* show that the aptamer immobilization leads to an increase in the surface roughness. The chemisorption of TNF to the aptamer leads to an increase in the threshold voltage (in the magnitude). The higher the concentration, the larger the change in the threshold voltage (Fig. 18 *a*). The current $I_{ds}$ is related to $V_t$ by Eqn (8). The change in $V_t$ leads to the corresponding change in $I_{ds}$. The change in the current $I_{ds}$ served as the analytical signal and was used to construct a calibration curve of the sensor (Fig. 18 *b*). The detection limit was in the concentration range characteristic

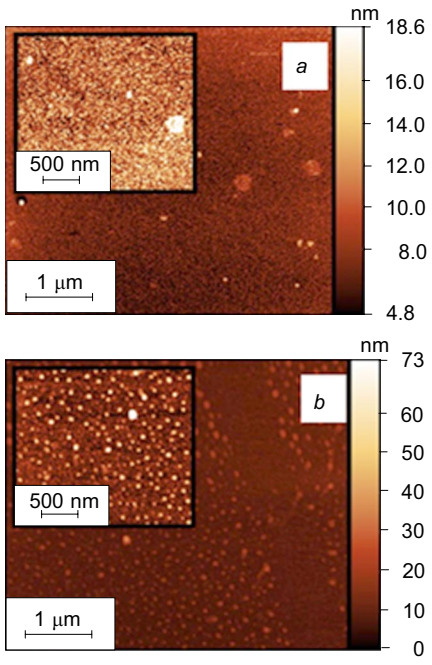



**Figure 17.** AFM images of the gold gate surface before (*a*) and after (*b*) aptamer immobilization.[11]

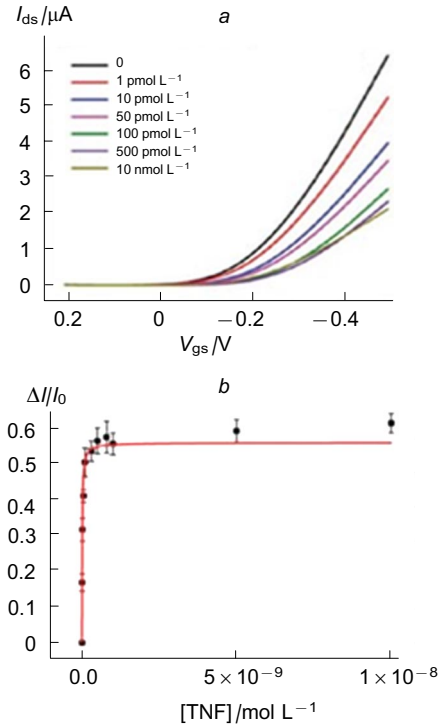



**Figure 18.** Transfer characteristics of the EGOFET sensor at different TNF concentrations in phosphate buffer (*a*) and the dose–response concentration curves at $V_{gs} = -0.5$ V (*b*).[11] The red line represents the approximation of the experimental data by the Langmuir equation.

of pathological TNF levels in the human body. Hence, this sensor can be employed in clinical practice. The authors stated that the chemisorption of TNF to the aptamer active sites is reversible because the transfer characteristics return to the initial values after washing of the sensor in phosphate buffer.

Piro *et al.*[59] developed a new immunosensor for the detection of bisphenol A (BPA), which is an important industrial chemical used in the manufacture of plastic commodity. When released to the environment, BPA can migrate and break the binding between estrogen and the appropriate receptor, thereby increasing cancer risk.[106] The schematics of the device and the principle of operation of the immunosensor are displayed in Fig. 19 *a*. In this device, the semiconductor layer was formed by poly[2,5-bis(3-tetradecylthiophen-2-yl)thieno[3,2-b]thiophene] (pBTTT) immobilized with 4-[2-(4-hexyloxyphenyl)prop-2-yl]phenol (alkyl-bisphenol A, $^{alk}$BPA) *via* co-crystallization. Antibodies (rabbit immunoglobulin G), capable of specifically binding to BPA, (hereinafter $AT_{BPA}$) were immobilized on the surface of the conducting channel. The addition of BPA led to the competition between $^{alk}$BPA, immobilized on the semiconductor, and bisphenol A in the solution, and a part of $AT_{BPA}$, being bound to BPA, was transferred to the solution, resulting in an increase in the current $I_{ds}$. The authors attributed this fact to an increase in the EDL capacitance. The sensing response ($\Delta I/\Delta I_{max}$) as a function of the BPA concentration in the incubation solution is shown in Fig. 19 *b*. The detection limit of BPA was ~2 pg mL$^{-1}$, which corresponds to the allowable level of stable contaminants in potable water.

Palazzo *et al.*[44] demonstrated that analyte molecules can be detected at distances longer than the Debye length $\lambda$. In

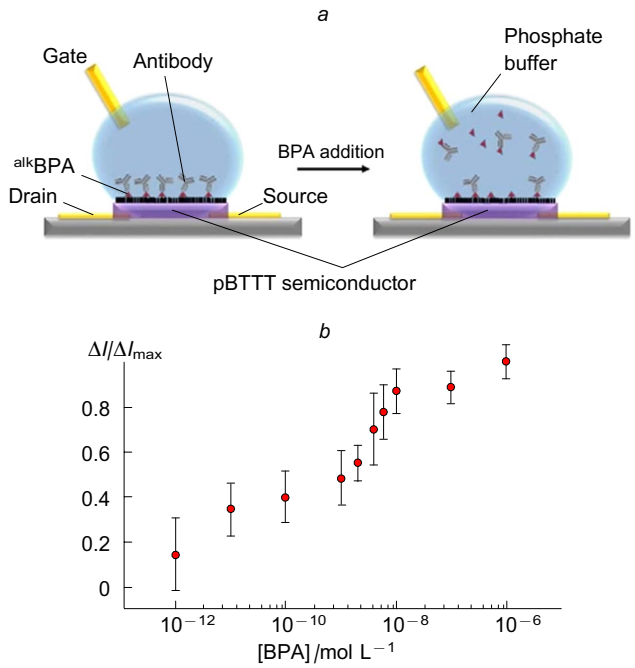



**Figure 19.** Schematics of the operation of the immunosensor (*a*) and the sensing signal $\Delta I/\Delta I_{max}$ as a function of the BPA concentration (*b*) at $V_{ds} = -0.45$ V, $V_{gs} = -0.6$ V.[59]

the context of biosensors $\lambda$ is the distance, at which charged analyte molecules can electrically interact with the surface of the receptor layer. If the charge is at a distance longer than $\lambda$, it is screened by ions of the solution. Therefore, some researchers reported that OFET sensors lose sensitivity if the Debye length is smaller than the distance required for molecular recognition.[54, 107] Therefore, this sensor can operate only at a low ionic strength of the solution, at which $\lambda$ is larger than the size of the analyte molecule. However, EGOT-based biosensors allowed the detection of the binding to the biorecognition layer of the analyte at a distance $\sim$30 times larger than $\lambda$, *i.e.*, the detection is possible, in particular, at high salt concentrations.

The authors studied this issue using an EGOT-based sensor, which is schematically shown in Fig. 20 *a*. The biorecognition layer consisted of three parts, which were formed as follows. One phospholipid layer was deposited on the P3HT semiconductor surface functionalized with COOH groups. The device was immersed in a streptavidin or avidin solution and then in a biotinylated solution of anti-CRP monoclonal antibodies. The anti-CRP monoclonal antibodies selectively interact with the C-reactive protein, which is a marker of different inflammatory processes in the body.[108]

The plots of the response *versus* the CRP concentration were constructed (Fig. 20 *b*) in order to explain the sensing mechanism. The relative change in the drain–source current was considered as the analytic signal

$$\frac{\Delta I}{I_0} = \frac{I_{ds} - I_0}{I_0} \tag{20}$$

where $I_0$ is the base line of $I_{ds}$ measured in the absence of the analyte. As can be seen in Fig. 20 *b*, the response increases with increasing CRP concentration. Hence, the response induced by the protein binding can be measured at a distance of 20–30 nm [*i.e.*, (30–40) $\lambda$] from the transistor channel.

Apparently, this can be explained as follow. The analytical signal of the sensor can be divided into two components

$$\frac{\Delta I}{I_0} = \frac{\Delta C}{C_0} + \frac{2\Delta V_t}{V_{gs} - V_{t,0}} \tag{21}$$

Since the binding of the analyte to the receptor occurs at a significant distance from the semiconductor layer, the charge mobility $\mu$ can be considered as a constant value. A comparison of the contributions of $V_t$ and $C$ [terms in Eqn (21)] to the analytical signal shows that the signal is largely determined by the capacitance change. Since immobilized proteins and appropriate counterions form an ionic liquid-like layer upon the formation of EDL, the Donnan equilibrium is established at the boundary of the immobilized ions.[109, 110] Therefore, the EGOT capacitance can be

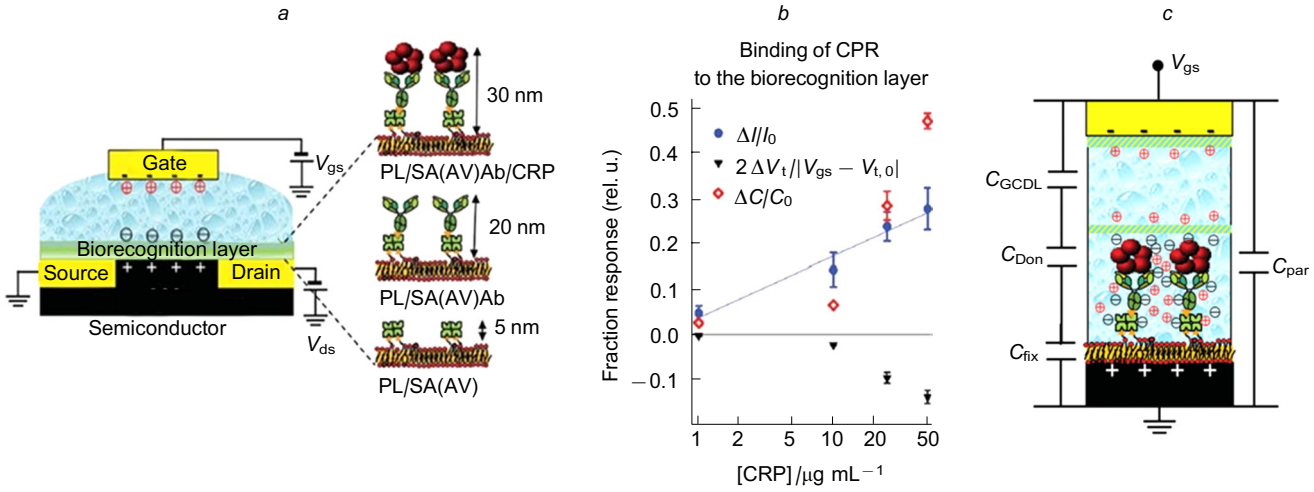



**Figure 20.** Schematics of the EGOFET device comprising three biorecognition layers on the organic semiconductor surface (*a*), the analytical signal change as a function of the C-reactive protein concentration in the solution (*b*) and schematic of the charge distribution in the receptor layer (*c*) (dashed regions indicate the positions of the ionic double layers; the equivalent scheme of sensor capacitances is presented).[44] PL is phospholipid, SA is streptavidin, AV is avidin, Ab is antibody, CRP is C-reactive protein.

represented as the following three components (the equivalent scheme is shown in Fig. 20 *c*):

— $C_{fix}$ determined by the dense part of EDL and the capacitance of the phospholipid layer,

— $C_{GCDL}$ is the capacitance of the diffuse EDL proportional to the square root of the ionic strength of the solution $i_s$ in the presence of the protein layer,

— the Donnan capacitance $C_{Don}$, directly proportional to $i_s$; the parallel capacitance $C_{par}$ was added to completely account for the assembled proteins.

According to the proposed model, the sensing response of the device is determined by the capacitance effect independent of the state in which the Donnan equilibrium is established and, consequently, independent of $\lambda$. Therefore, it was demonstrated that EGOT-based sensors can operate in the presence of high concentrations of the non-detected components in the analyte solution ($\lambda = 0.7$ nm). In order to confirm this concept, successful measurements were performed in the blood serum.

Therefore, the fabrication of EGOFET- and OECT-based biosensors has attracted great attention in the field of organic electronics. The above examples demonstrate that the detection limits of these devices are comparable with the detection limits of methods employed in clinical practice. The advantages of biosensors based on electrolyte-gated transistors are that they are portable, inexpensive and easy to handle, due to which they can be used not only in clinical practice but also at the patient's bedside, which significantly extends the diagnostic potential of modern medicine.

### 5.2. Chemical sensors

The number of publications on the application of EGOTs as chemical sensors is much smaller compared to those devoted to their use as biosensors. This is due to the fact that the main advantage of EGOTs is that they operate in a low voltage range, which is of importance for the analysis of biological molecules, while other simple and well-developed procedures are available for chemical analysis.[111] Nevertheless, EGOT-based sensors are characterized by high sensitivity and rapid response and can be used in *in situ* assays in biological media. Hence, these sensors are applied, in particular, for the quantitative analysis of aqueous solutions for the presence of ions[33, 50, 60] or gases[53] and also as pH sensors.[63, 112]

Let us consider practical applications of EGOFETs as chemical sensors. Nguyen *et al.*[33] reported the use of EGOFET for the detection of $Cu^{2+}$ ions in solutions. The schematic of this sensor is shown in Fig. 21 *a*. Poly(*N*-diketopyrrolopyrrole dithienylthieno[3,2-*b*]thiophene) deposited by spin coating was employed as the semiconductor layer. The Gly–Gly–His tripeptide, which selectively interacts with $Cu^{2+}$ ions in solution to form a complex compound, was immobilized on the gold gate. It was noted that the protein-modified gate electrode of this sensor can be utilized many times. The formation of a copper complex leads to a significant threshold voltage shift and a change in $I_{ds}$ (Fig. 21 *b*,*c*). The weak effect of small impurities of other ions and substances on the performance of the sensor was demonstrated by measurements for specially prepared water and regular tap water without additional distillation or

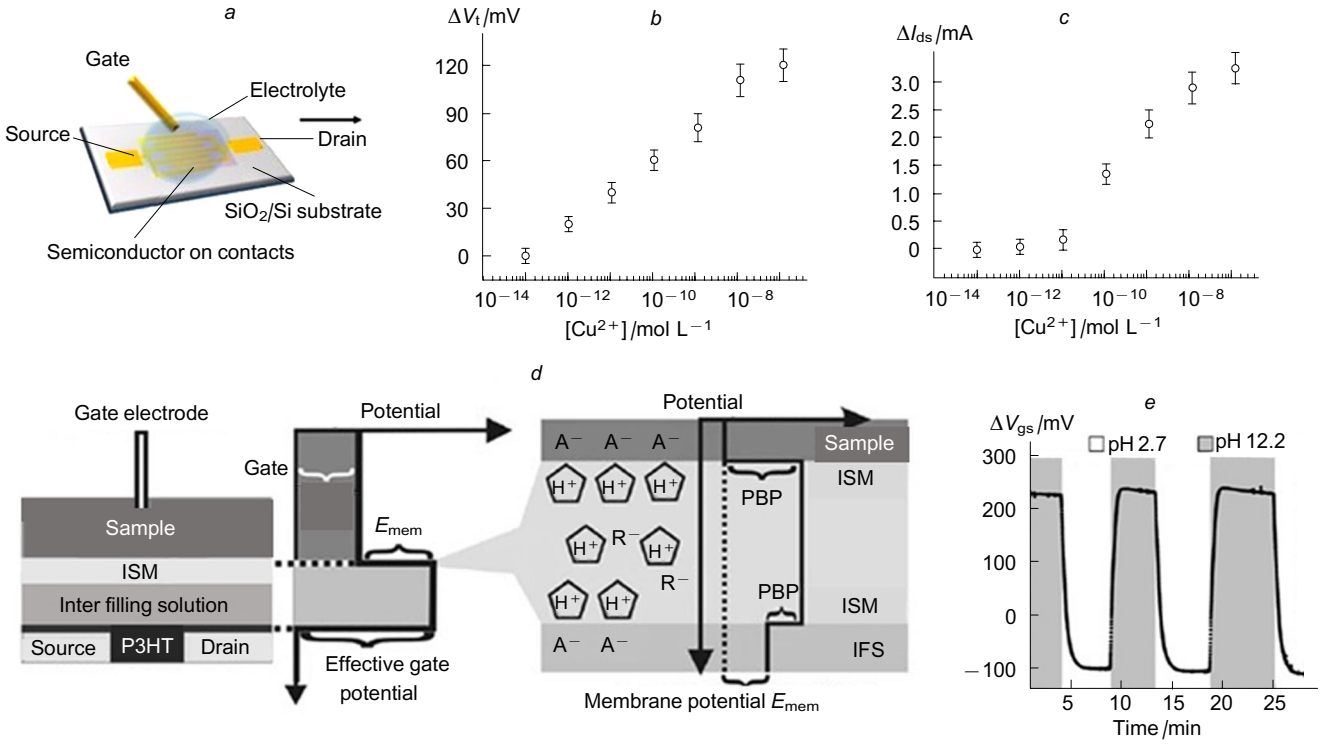



**Figure 21.** Schematics of the EGOFET sensor for $Cu^{2+}$ ions (*a*),[33] threshold voltage shift (*b*) and current change (*c*) as a function of the concentration of $Cu^{2+}$ ions in water; schematics of the operation mechanism of the ion-selective EGOFET-based pH sensor (*d*); threshold voltage shift as a function of time during a periodic variation of the pH value from pH 12.2 to pH 2.7 (*e*).[12] PBP is the Nernstian phase boundary potential, IFS is the internal filling solution, $H^+$ are hydrogen ions, $A^-$ are anions in the solution, $R^-$ are anions of the membrane, ISM is the ion-selective membrane.

purification. The detection limits were $5 \times 10^{-13}$ and $5 \times 10^{-11}$ mol $L^{-1}$ in the measurements based on the threshold voltage shift and the current change, respectively. It was emphasized that the functionalization of the gate electrode with an appropriate ionophore makes it possible to detect other ions. Hence, this sensor can be considered as a universal device.

The development of pH sensors based on organic semiconductors, in particular EGOFETs and OECTs, has attracted great attention. Alam *et al.*[62] published a comprehensive review on organic materials for different types of pH sensors, the fabrication of devices based on these materials and their application in medicine. Kofler *et al.*[112] designed an ion-selective EGOT for the measurement of pH values in the range from pH 2.7 to pH 12.2. The schematics of the sensor and its operation mechanism are presented in Fig. 21 *d*. In this sensor, P3HT served as the semiconductor material. A polydimethylsiloxane reservoir was placed on the semiconductor surface and filled with 0.2 M phosphate buffer, pH 7, as the inner filling solution (IFS). The polymeric ion-selective membrane (ISM), which was fabricated by a procedure described Liu *et al.*,[113] was sandwiched between the reservoir and the flow cell. The effective potential at the gate was represented as the sum of the gate potential and the membrane potential ($E_{mem}$), which was expressed by two Nernstian phase boundary potentials (PBPs) — at the ISM/IFS and sample/ISM interfaces. Each potential depends on the corresponding pH values. The sensing response was determined from the potential drop at ISM (membrane potential), which depends on the pH according to the Nernstian equation

$$E_{mem} = E_0 + \frac{RT}{z_i F}\frac{pH_s}{pH_{is}} \quad (22)$$

where $E_0$ is the constant, $R$ the universal gas constant, $z_i$ is the charge of the analyte ion, F is the Faraday constant, $pH_s$ is the pH of the sample and $pH_{is}$ is the pH of the inner filling solution.

The sensing signal as a function of the time measured during periodic variation of the pH value is presented in Fig. 21 *e*. According to this dependence, even long continuous measurements of up to 30 min did not show any degradation of the device. The advantage of the proposed pH sensor over standard glass electrode is that it can be employed in bioassays for *in vivo* measurements of pH of the blood. In other studies, the authors demonstrated that ion-selective EGOTs can be applied to detect $Na^+$ ions in a wide concentration range[60] and investigated the effect of the ionic strength of the solution and the operation regime of the device on its stability.[91, 114]

Werkmeister and Nickel[53] created an EGOFET-based sensor for the detection of ammonia in aqueous solutions. Dinaphtho[2,3-*b*:20,30-*f*]thieno[3,2-*b*]thiophene served as the semiconductor. Ammonia is the end product of amino acid degradation. It is highly toxic and is present in biological fluids in the human body in low concentrations; the major part of ammonia is converted to urea.[75] The sensor described by the authors[53] allows the detection of ammonia down to the concentration of 0.1 mmol $L^{-1}$, which corresponds to the blood ammonia level in patients with severe diseases (the normal concentration is lower than 0.05 mmol $L^{-1}$).

Bao and co-workers[50] developed a procedure for the detection of mercury ions in seawater even in the presence of high background concentrations of salts. Mercury ions are very environmentally hazardous because they can be accumulated in organs of living organisms and are inhibitors of some enzymes, *e.g.*, of thioredoxin reductase involved in the biosynthesis of vitamins.[115] A layer sensitive to mercury ions was created by the deposition of gold nanoparticles on the semiconductor surface (the structure is considered in Section 4) followed by the deposition of thiolated DNA aptamer, which, as demonstrated above, can specifically bind to $Hg^{2+}$ ions.[116] This method allowed the detection of $Hg^{2+}$ at concentrations of 10 μmol $L^{-1}$.

The above examples demonstrate that EGOT-based devices are promising chemical sensors for aqueous and biological media.

### 5.3. Neuromorphic devices

A promising application of EGOT is the design of neuromorphic devices. These are systems mimicking the biologic architecture of neurons forming the nervous system. The main drawback of current computing devices based on the von Neumann architecture, known as the von Neumann bottleneck, is the physical separation of the memory and the processor. In the human brain, they are merged, which allows the simultaneous processing of information due to the ability of interconnected neurons to change their properties with time in response to local changes (plasticity). Hence, the integration of neurons and synaptic connections is required for the creation of a brain-like computer.[27] The design of NOMFET (nanoparticle organic memory field-effect transistor) as a memory unit based on OFETs and nanoparticles provides an approach to the implementation of computation and memory in a single device.[27] These devices exhibit short-term synaptic plasticity due to a combination of two properties of NOMFET — the transconductance gain of the transistor and the memory effect. The memory effect is associated with the charge of nanoparticles (generally, gold nanoparticles), which act as nanoscale capacitors embedded into a semiconductor (Fig. 22 *a*).

The transconductance of a transistor can be dynamically tuned depending on the amount of charges in nanoparticles. This is used to implement the time-dependent synaptic weight (*i.e.*, signal transmission activity). The basic function of the synapse is described by pre- and postsynaptic signals, specified by the drain – source voltage and current of the NOMFET. The dynamic behaviour of the device in the frequency range from 0.01 to 10 Hz can be tailored by adjusting the size of nanoparticles (from 5 to 20 nm) and the channel length of the transistor. Alibart *et al.*[27] noted that the functional model of NOMFET as the simplest synapse can be obtained by the exponential approximation of the relaxation function of nanoparticle discharge.

The above-described working principle of artificial synapses is of interest not only for the creation of computing systems but also for the bioelectronic applications. To interface with neuronal cells and for recording and transduction of bioelectric signals from cells and tissues, the device, as in the case of biosensors, should operate at low voltages. Desbief *et al.*[22] suggested using an electrolyte-gated organic synapstor, the schematic of which is presented in Fig. 22 *b*, for the prosthesis application — the replacement of lacking chemical synapses between adjacent cells with electrical synapses. In this case, the mechanism of signal transduction of the electrolyte-gated synapstor is similar to the working mechanism of the above NOMFET. However, the synapstor uses an electrolyte gate, making it possible to operate in the voltage range down to one volt. A

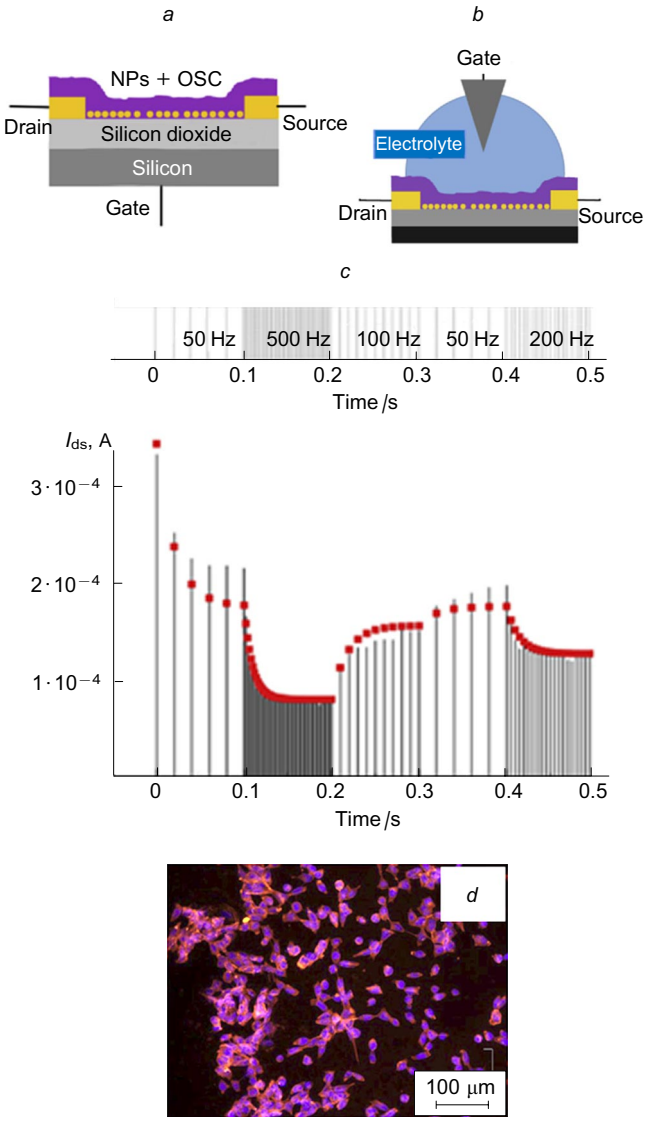



**Figure 22.** Schematics of the NOMFET device (*a*) and the electrolytic synapstor (*b*); short-term synaptic response of the electrolytic synapstor in a water salt solution (the spike voltage is 50 mV, red points correspond to the values calculated from the model described Alibart *et al.*[27]) (*c*), optical image of SH-SY5Y cells cultured on pentacene (*d*).[22] OSC is organic semiconductor.

0.1 M aqueous NaCl solution was employed as the electrolyte, and a 40 nm thick pentacene layer, with embedded gold nanoparticles 10 nm in diameter, served as the semiconductor. When changing the frequency of the input signal, the authors observed the behaviour of the device similar to that of a biological synapse: the depressing behaviour (decrease of the output signal; drain – source current) and facilitating behaviour (increase of the output signal) (see Fig. 22 *c*). To assess the biocompatibility of the substrate, human neuroblastoma stem cells SH-SY5Y and NE-4C were adhered to the pentacene films in the fabricated devices and differentiated into neuronal phenotypes, which was confirmed by the specific reaction with β-III-tubulin (Fig. 22 *d*). The presence of neurons on the surface of the device was shown to have no significant effect on the properties of the latter. Therefore, the electrolyte-gated synapstors can be used for the prosthesis of synaptic connections. The problem to be solved is that the addition of gold nanoparticles leads to an increase in the roughness of the semiconductor surface and a decrease in the transconductance of the electrolyte-gated transistor.

Cramer *et al.*[24] reported the use of EGOFETs for the stimulation and recording of signals of the murine stem cell-derived neuronal network. The cell cultures of the murine neural NE-4C stem cell line and its GFP-NE-4C clone were grown and differentiated on the fabricated EGOFETs according to the protocol published in the study.[117] The schematic and the photograph of the device are shown in Fig. 23 *a* and *b*, respectively. The 9 nm thick pentacene film deposited by high vacuum sublimation served as the semiconductor layer. The procedure of the fabrication of the device was described in detail Shehu *et al.*[118] A polystyrene pool to confine the cell culture was attached to the top of the pentacene film; platinum wire was used as the gate electrode. The AFM image of the pentacene film surface and the schematic of the sensing areas and contacts in the device are shown in Fig. 23 *c*. Four interdigitated source-drain electrodes were fabricated on one substrate, two of which were for signal recording and the other two were for the stimulation of the cell culture. It was noted that the device showed high performance stability in an aqueous medium even in the absence of an additional protective layer.

The device response was recorded during different phases of the neuronal differentiation for 9 days. The epifluorescence microscope image of the neuronal network on the surface of the device obtained on the eighth day of the incubation is presented in Fig. 23 *d*. To confirm the differentiation of stem cells into neurons, β-III-tubulin was stained red using immunofluorescence labels; the cell nuclei and GFP-NE-4C cells were stained blue and green, respectively. It is clearly seen that the majority of stem cells were differentiated into neurons and formed a neuronal network on the surface of the device, as evidenced by a large red-stained area in the fluorescence microscope image.

Cramer *et al.*[24] reported that, when a population of neurons is obtained, the interconnected neuronal network can be stimulated and collective bioelectric signals can be recorded. This is evidence that the device is sensitive to signals elicited by neurons but not by undifferentiated stem cells. This behaviour is not only important for interfacing or implanting transducers of neuronal signals and for electrical stimulation, but is also attractive in stem cell-based therapies for spinal cord injury. In the latter case, a minimally-invasive device with capabilities to electrically stimulate and monitor neuronal plasticity is required. Therefore, EGOFETs based on ultrathin pentacene films can be considered as a promising platform for transducers of neuronal activity.

Lenz *et al.*[25] proposed the vertical architecture for the fabrication of a nanoscopic EGOT (Fig. 24 *a*) and demonstrated that it can be employed in neuromorphic computers operating at low voltages. The authors emphasized that this device holds promise due to its high performance characteristics (the $I_{on/off}$ ratio is $10^8$ and the current density is 3 mA $cm^{-2}$) and a low contact resistance, thereby enabling the device to operate at high frequencies. One of the main advantages of the vertical architecture is a decrease in the size of EGOT. Thus, the device has a channel length of $<50$ nm and a footprint of $2 \times 80 \times 80$ nm, which makes it possible to integrate this device onto various chips.

The schematic and the SEM image of the fabricated device are presented in Fig. 24 *a*,*b*. A 2 nm thick layer of the diketopyrrolopyrrole – terthiophene donor – acceptor polymer (PDPP) was used as the organic semiconductor. This

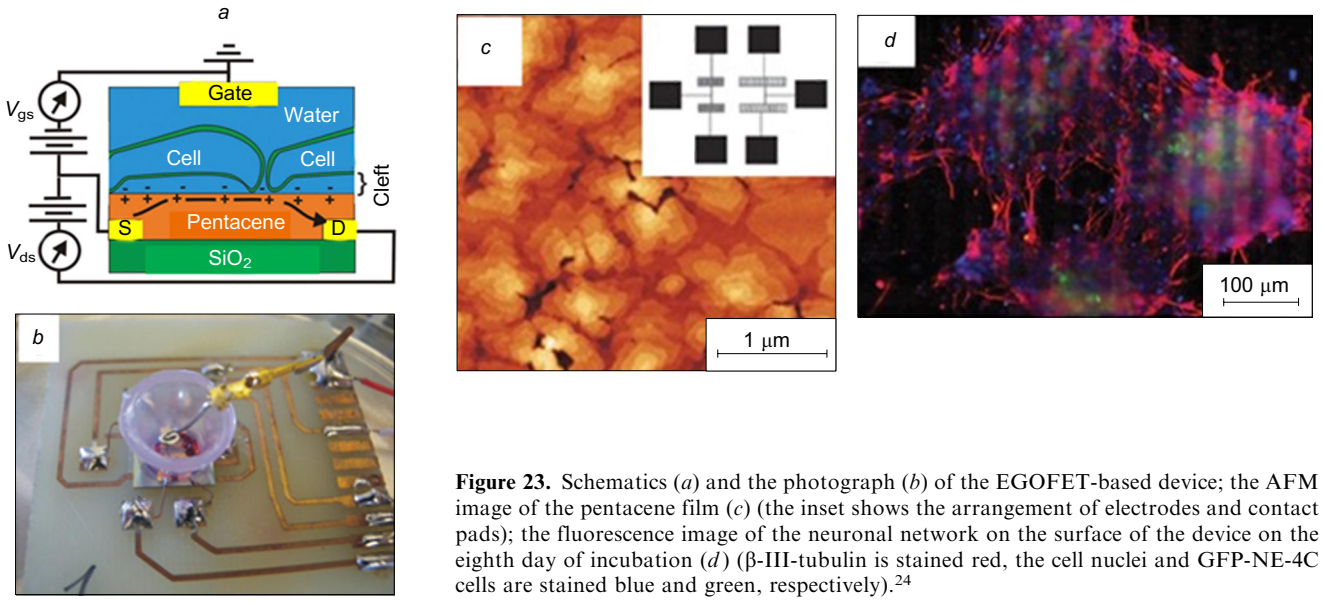



**Figure 23.** Schematics (*a*) and the photograph (*b*) of the EGOFET-based device; the AFM image of the pentacene film (*c*) (the inset shows the arrangement of electrodes and contact pads); the fluorescence image of the neuronal network on the surface of the device on the eighth day of incubation (*d*) (β-III-tubulin is stained red, the cell nuclei and GFP-NE-4C cells are stained blue and green, respectively).[24]

polymer was deposited by spin coating. The ionic liquid 1-ethyl-3-methylimidazolium bis(trifluoromethylsulfonyl)imide ([EMIM][TFSI]) served as the electrolyte.

To prove the applicability of vertical EGOTs for the design of neuromorphic computing systems, the authors demonstrated the artificial synaptic behaviour of the EGOT with short- and long-term plasticity. As previously reported,[119] there is an analogy between the electrolyte/semiconductor interface and the presynaptic part of the chemical synapse and also between the drain – semiconductor – source transition as the postsynaptic part. The appearance of postsynaptic spikes was attributed to the injection of electrolyte ions to the organic semiconductor on application of an electrical pulse to the gate electrode and the subsequent return of the ions to the solution. The plots of the excited postsynaptic drain – source current as a function of time, presented in Fig. 24 *c*,*d*, show that the EGOT can be employed as an artificial synapse. Since after the first pulse, ions have no time to return to the solution, the subsequent signal is enhanced, *i.e.*, in the authors' opinion, a short-term neuronal plasticity appears (see Fig. 24 *c*). In particular, after the application of two presynaptic spikes (100 ms) with an inter-spike interval of 1 s ($V_{gs}$ = −1.2 V, $V_{ds}$ = −0.1 V), a signal as a pair of postsynaptic spikes with amplitudes of 10.5 and 608 μA were recorded. The long-term plasticity was triggered by six successive pulses with an amplitude of −0.8 V, a pulse duration of 50 ms and an inter-spike interval of 2.5 s. The authors observed a significant increase in the drain – source current (see Fig. 24 *d*), which was interpreted as the appearance of

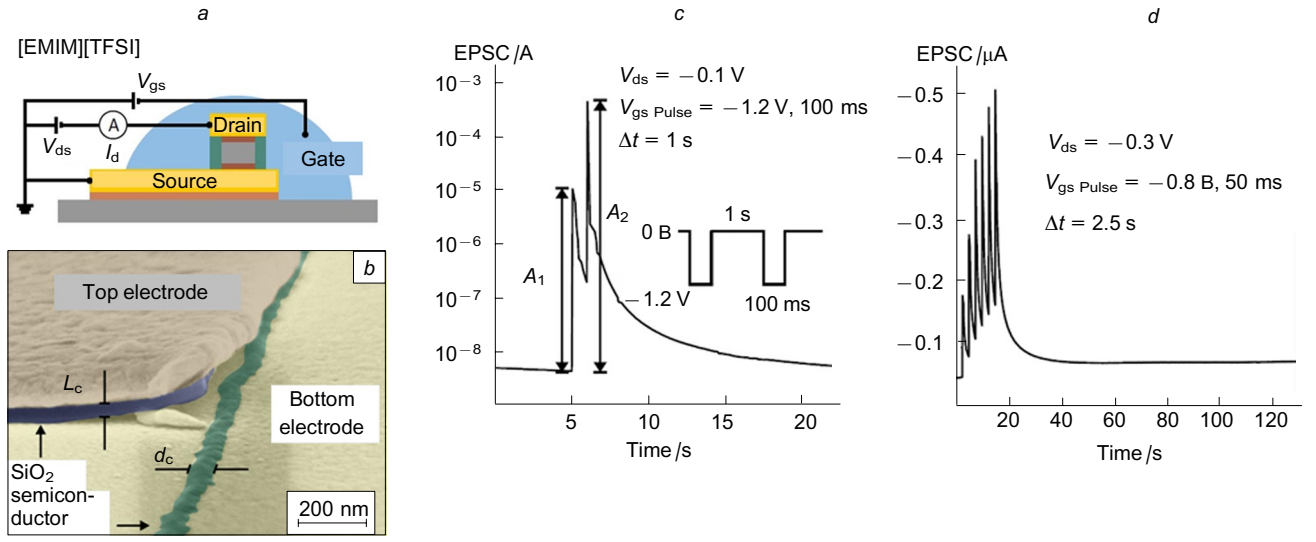



**Figure 24.** Schematics of the vertical EGOT (*a*), the colored SEM image of the vertical lateral section of the EGOT (*b*), excitatory postsynaptic current (EPSC) as a function of time triggered by two pre-synaptic spikes (−1.2 V, 100 ms) with a step of 1 s (short-term plasticity) (*c*) and six pulses (−0.8 V, 50 ms) with a step of 2.5 s (long-term plasticity) (*d*).[25]
(*a*) Gold involved in the electrodes is yellow, the titanium sublayer is dark-brown, the chromium sublayer is pale-brown, the semiconductor is green, the electrolyte [EMIM][TFSI] is blue; (*b*) two gold electrodes are yellow, the $SiO_2$ layer is blue, the PDPP semiconductor layer is green, $L_c$ is the channel length, $d_c$ is the channel width; (*c*) $A_1$ and $A_2$ are the amplitudes of the first and second postsynaptic responses, respectively.

long-term plasticity and the memory formation. The minimum energy required for a switching operation was in the range of $10^{-13}$ – $10^{-14}$ J ($V_{ds}$ = 100 μV and $V_{gs}$ = −0.4 to −1.2 V), which is smaller than the corresponding value in devices based on metal – oxide – semiconductor complementary structures and is only an order of magnitude larger than the energy of switching in the brain. High stability of the device is worthy of note. Thus, after three months of storage in a desiccator; the EGOT showed only small shifts in the threshold voltage and insignificant changes in the on current. The device can operate in the continuous current mode without significant degradation for at least 50 min. Lenz *et al.*[25] suggested that high stability of the architecture of OECT proposed in their study stems from the device geometry optimal for acting as a heat sink for rapid dissipation of heat.

The above examples show that EGOFETs and OECTs are a promising platform for neuromorphic computing systems mimicking the ability of the human brain to learning and training and also for transducers of neuronal activity. An important feature of electrolyte-gated transistors is biocompatibility.[103] Hence, such transistors can be employed as artificial synapses, which can serve as prostheses to restore synaptic connections.

## 6. Conclusion

In recent years, significant progress has been made in the field of electrolyte-gated organic transistors. Researchers succeeded in improving their key electrical parameters, achieving high stability and repeatability of the devices and significantly expanding the area of their application. It is worth noting that electrolyte-gated organic transistors came into use as artificial synapses quite recently and this area is currently at an early stage of the development, while the method based on EGOTs as sensors for the detection of biological molecules and chemical substances is already competitive in sensitivity with modern appropriate techniques (*e.g.*, immunoenzymatic assay). Meanwhile, the advantage of EGOT-based sensors it that they can be employed in field conditions.

Electrolyte-gated organic transistors are currently widely used for the detection of different analytes, from ions of inorganic compounds to large biologically active molecules. One direction of the further development of this field is the creation of arrays of EGOT sensors sensitive to different analyte molecules as electronic tongue systems. The electronic tongue is a tool based on an array of nonspecific, low-selective sensors and an appropriate method of mathematical processing of a multidimensional array of responses. This tool allows the creation of 'fingerprints' of each analyte and can be considered as a promising device in the quantitative and qualitative analysis.[120] Pioneering works on electronic tongue systems were performed back in the 1990s and these systems were fabricated employing different types of sensors, such electrochemical (potentiometric, amperometric, voltammetric), optical and impedimetric sensors and also enzymatic biosensors.[121 – 123] Electronic tongue systems can be used, *e.g.*, in the food and beverage safety certification.[124 – 127] Highly sensitive EGOT sensors significantly extend the potential of the electronic tongue, in particular, for medicinal purposes, in screening and diagnostic methods.

Another potential field of application of EGOT-based sensors is the highly demanded lab-on-chip technology, widely researched in recent years. The lab-on-chip technology integrates all the functions of a traditional test laboratory, including transferring samples, drawing off a precise volume of the sample and assaying with a system of a few square centimetres.[128] The lab-on-chip employs microfluidic systems, which allow the precise delivery of small amounts of a solution to a detection chamber containing several sensors, thereby making it possible to simultaneously detect several analytes with a portable and easy-to-use device.[59] Sensors based on EGOTs can be employed in laboratory-on-chip systems, because they possess such properties as portability and simplicity combined with high sensitivity and selectivity.

An important factor favourable for the development of these fields of application of EGOT sensors is the extension of the range of semiconductors for the fabrication of EGOTs. Currently, most of researchers dealing with the development of EGOT sensors employ a limited number of commercially available semiconductors. The design, manufacturing and commercialization of semiconductors, specially developed for the use in aqueous media can significantly improve the performance characteristics of EGOTs and facilitate the market entry of devices based on such semiconductors, similar to the emerging area of materials for photovoltaics.[129 – 132]

In the fundamental research on electrolyte-gated organic transistors, there are issues that remained to be solved, such as the mechanisms of conduction in EGOFETs and OECTs and the mechanisms of changes in the electrical characteristics related to the sensing response or synaptic plasticity. The thorough investigation of these mechanisms should facilitate the further development of this area of research.

Figures 2 *a*,*b*, 4 – 6, 12, 17, 18, 20 are courtesy of Wiley and Sons; Figs 2 *c*,*d*, 15, 16, 21 *d*,*e* are courtesy of AIP Publishing; Figs 3,*b*,*c*, 11, 24 are courtesy of Springer Nature; Fig. 9 is courtesy of IOP Publishing; Figs. 13, 14, 19, 21 *a* – *c*, 22 are courtesy of Elsevier; Fig. 23 is courtesy of Royal Society of Chemistry; Fig. 10 is courtesy of the Korean Physical Society.

The review was prepared within the framework of the state assignment (Sections 2, 4, 5.3) and was supported by the Russian Science Foundation (Project No. 19-73-30028, Sections 1, 3, 5.1, 5.2).

## References

1. L.Torsi, M.Magliulo, K.Manoli, G.Palazzo. *Chem. Soc. Rev.*, **42**, 8612 (2013)
2. J.Rivnay, S.Inal, A.Salleo, R.M.Owens, M.Berggren, G.G.Malliaras. *Nat. Rev. Mater.*, **3**, 17086 (2018)
3. T.Cramer, A.Campana, F.Leonardi, S.Casalini, A.Kyndiah, M.Murgia, F.Biscarini. *J. Mater. Chem. B*, **1**, 3728 (2013)
4. P.Bergveld. *IEEE Trans. Biomed. Eng.*, **17**, 70 (1970)
5. P.Bergveld. *Sens. Actuators, B*, **88**, 1 (2003)
6. J.C.Cooper, E.A.H.Hall. *J. Biomed. Eng.*, **10**, 210 (1988)
7. T.Sakata. *ACS Omega*, **4**, 11852 (2019)
8. S.Casalini, F.Leonardi, T.Cramer, F.Biscarini. *Org. Electron.*, **14**, 156 (2013)
9. M.Berto, E.Vecchi, L.Baiamonte, C.Condò, M.Sensi, M.Di Lauro, M.Sola, A.De Stradis, F.Biscarini, A.Minafra, C.A.Bortolotti. *Sens. Actuators, B*, **281**, 150 (2019)
10. P.Seshadri, K.Manoli, N.Schneiderhan-Marra, U.Anthes, P.Wierzchowiec, K.Bonrad, C.Di Franco, L.Torsi. *Biosens. Bioelectron.*, **104**, 113 (2018)
11. M.Berto, C.Diacci, R.D'Agata, M.Pinti, E.Bianchini, M.Di Lauro, S.Casalini, A.Cossarizza, M.Berggren, D.Simon, G.Spoto, F.Biscarini, C.A.Bortolotti. *Adv. Biosyst.*, **2**, 1700072 (2018)

12. E.MacChia, A.Tiwari, K.Manoli, B.Holzer, N.Ditaranto, R.A.Picca, N.Cioffi, C.Di Franco, G.Scamarcio, G.Palazzo, L.Torsi. *Chem. Mater.*, **31**, 6476 (2019)
13. C.Diacci, M.Berto, M.Di Lauro, E.Bianchini, M.Pinti, D.T.Simon, F.Biscarini, C.A.Bortolotti. *Biointerphases*, **12**, 05F401 (2017)
14. S.J.Park, O.H.Kwon, S.H.Lee, H.S.Song, T.H.Park, J.Jang. *Nano Lett.*, **12**, 5082 (2012)
15. L.T.E.Macchia, P.Romele, K.Manoli, M.Ghittorelli, M.Magliulo, Z.M.Kovács-Vajna, F.Torricelli, L.Torsi. *Flex. Print. Electron.*, **3**, 034002 (2018)
16. M.Berto, S.Casalini, M.Di Lauro, S.L.Marasso, M.Cocuzza, D.Perrone, M.Pinti, A.Cossarizza, C.F.Pirri, D.T.Simon, M.Berggren, F.Zerbetto, C.A.Bortolotti, F.Biscarini. *Anal. Chem.*, **88**, 12330 (2016)
17. S.Ricci, S.Casalini, V.Parkula, M.Selvaraj, G.D.Saygin, P.Greco, F.Biscarini, M.Mas-Torrent. *Biosens. Bioelectron.*, **167**, 112433 (2020)
18. W.Huang, A.K.Diallo, J.L.Dailey, K.Besar, H.E.Katz. *J. Mater. Chem. C*, **3**, 6445 (2015)
19. K.Hong, S.H.Kim, A.Mahajan, C.D.Frisbie. *ACS Appl. Mater. Interfaces*, **6**, 18704 (2014)
20. R.A.Picca, K.Manoli, E.Macchia, L.Sarcina, C.Di Franco, N.Cioffi, D.Blasi, R.Österbacka, F.Torricelli, G.Scamarcio, L.Torsi. *Adv. Funct. Mater.*, **30**, 1904513 (2019)
21. Y.Lee, T.-W.W.Lee. *Acc. Chem. Res.*, **52**, 964 (2019)
22. S.Desbief, M.Di Lauro, S.Casalini, D.Guerin, S.Tortorella, M.Barbalinardo, A.Kyndiah, M.Murgia, T.Cramer, F.Biscarini, D.Vuillaume. *Org. Electron.*, **38**, 21 (2016)
23. A.Kyndiah, F.Leonardi, C.Tarantino, T.Cramer, R.Millan-Solsona, E.Garreta, N.Montserrat, M.Mas-Torrent, G.Gomila. *Biosens. Bioelectron.*, **150**, 111844 (2020)
24. T.Cramer, B.Chelli, M.Murgia, M.Barbalinardo, E.Bystrenova, D.M.De Leeuw, F.Biscarini. *Phys. Chem. Chem. Phys.*, **15**, 3897 (2013)
25. J.Lenz, F.del Giudice, F.R.Geisenhof, F.Winterer, R.T.Weitz. *Nat. Nanotechnol.*, **14**, 579 (2019)
26. V.Parkula, M.S.Maglione, S.Casalini, Q.Zhang, P.Greco, C.A.Bortolotti, C.Rovira, M.Mas-Torrent, F.Biscarini. *Adv. Electron. Mater.*, **5**, 1800875 (2019)
27. F.Alibart, S.Pieutin, D.Guérin, C.Novembre, S.Lenfant, K.Lmimouni, C.Gamrat, D.Vuillaume. *Adv. Funct. Mater.*, **20**, 330 (2010)
28. Y.Van De Burgt, A.Melianas, S.T.Keene, G.Malliaras, A.Salleo. *Nat. Electron.*, **1**, 386 (2018)
29. L.Kergoat, L.Herlogsson, D.Braga, B.Piro, M.C.Pham, X.Crispin, M.Berggren, G.Horowitz. *Adv. Mater.*, **22**, 2565 (2010)
30. D.Wang, V.Noël, B.Piro. *Electronics*, **5**, (1), 9 (2016)
31. J.Liao, H.Si, X.Zhang, S.Lin. *Sensors (Switzerland)*, **19**, 352 (2019)
32. K.Manoli, M.Magliulo, M.Y.Mulla, M.Singh, L.Sabbatini, G.Palazzo, L.Torsi. *Angew. Chem., Int. Ed.*, **54**, 12562 (2015)
33. T.K.Nguyen, H.V.Tran, T.T.Vu, S.Reisberg, V.Noël, G.Mattana, M.C.Pham, B.Piro. *Biosens. Bioelectron.*, **127**, 118 (2019)
34. Y.Xia, D.Frisbie. In *Organic Electronics II: More Materials and Applications*. (Ed. H.Klauk). (Wiley-VCH Verlag, 2012). P. 198
35. T.Cramer, A.Kyndiah, M.Murgia, F.Leonardi, S.Casalini, F.Biscarini. *Appl. Phys. Lett.*, **100**, 143302 (2012)
36. Q.Zhang, F.Leonardi, S.Casalini, I.Temiño, M.Mas-Torrent. *Sci. Rep.*, **6**, 39623 (2016)
37. B.Nketia-Yawson, G.D.Tabi, Y.-Y.Noh. *ACS Appl. Mater. Interfaces*, **11**, 17610 (2019)
38. L.Fillaud, T.Petenzi, J.Pallu, B.Piro, G.Mattana, V.Noel. *Langmuir*, **34**, 3686 (2018)
39. A.Malti, E.O.Gabrielsson, M.Berggren, X.Crispin. *Appl. Phys. Lett.*, **99**, 100 (2011)
40. Q.Thiburce, A.J.Campbell. *Adv. Electron. Mater.*, **3**, 1600421 (2017)
41. H.Sinno, S.Fabiano, X.Crispin, M.Berggren, I.Engquist. *Appl. Phys. Lett.*, **102**, 113306 (2013)
42. A.S.Sizov, E.V.Agina, S.A.Ponomarenko. *Russ. Chem. Rev.*, **87**, 1226 (2018)
43. L.Kergoat, B.Piro, M.Berggren, G.Horowitz, M.C.Pham. *Anal. Bioanal. Chem.*, **402**, 1813 (2012)
44. G.Palazzo, D.De Tullio, M.Magliulo, A.Mallardi, F.Intranuovo, M.Y.Mulla, P.Favia, I.Vikholm-Lundin, L.Torsi. *Adv. Mater.*, **27**, 911 (2015)
45. F.Leonardi, S.Casalini, Q.Zhang, S.Galindo, D.Gutiérrez, M.Mas-Torrent. *Adv. Mater.*, **28**, 10311 (2016)
46. R.Colucci, H.F.D.P.Barbosa, F.Günther, P.Cavassin, G.C.Faria. *Flex. Print. Electron.*, **5**, 013001 (2020)
47. A.Laiho, L.Herlogsson, R.Forchheimer, X.Crispin, M.Berggren. *Proc. Natl. Acad. Sci. USA*, **108**, 15069 (2011)
48. B.G.Horowitz. *Adv. Mater.*, **5**, 365 (1998)
49. J.Zaumseil, H.Sirringhaus. *Chem. Rev.*, **107**, 1296 (2007)
50. O.Knopfmacher, M.L.Hammock, A.L.Appleton, G.Schwartz, J.Mei, T.Lei, J.Pei, Z.Bao. *Nat. Commun.*, **5**, 2954 (2014)
51. M.Di Lauro, M.Berto, M.Giordani, S.Benaglia, G.Schweicher, D.Vuillaume, C.A.Bortolotti, Y.H.Geerts, F.Biscarini. *Adv. Electron. Mater.*, **3**, 1700159 (2017)
52. K.Melzer, M.Brändlein, B.Popescu, D.Popescu, P.Lugli, G.Scarpa. *Faraday Discuss.*, **174**, 399 (2014)
53. F.X.Werkmeister, B.A.Nickel. *Org. Electron.*, **39**, 113 (2016)
54. M.L.Hammock, O.Knopfmacher, B.D.Naab, J.B.H.Tok, Z.Bao. *ACS Nano*, **7**, 3970 (2013)
55. A.Giovannitti, D.T.Sbircea, S.Inal, C.B.Nielsen, E.Bandiello, D.A.Hanifi, M.Sessolo, G.G.Malliaras, I.McCulloch, J.Rivnay. *Proc. Natl. Acad. Sci. USA*, **113**, 12017 (2016)
56. M.J.Donahue, A.Williamson, X.Strakosas, J.T.Friedlein, R.R.McLeod, H.Gleskova, G.G. Malliaras. *Adv. Mater.*, **30**, 1705031 (2018)
57. C.B.Nielsen, A.Giovannitti, D.T.Sbircea, E.Bandiello, M.R.Niazi, D.A.Hanifi, M.Sessolo, A.Amassian, G.G.Malliaras, J.Rivnay, I.McCulloch. *J. Am. Chem. Soc.*, **138**, 10252 (2016)
58. T.P.Nguy, R.Hayakawa, V.Kilinc, M.Petit, J.M.Raimundo, A.Charrier, Y.Wakayama. *Jpn. J. Appl. Phys.*, **58**, SDDH02 (2019)
59. B.Piro, D.Wang, D.Benaoudia, A.Tibaldi, G.Anquetin, V.Noël, S.Reisberg, G.Mattana, B.Jackson. *Biosens. Bioelectron.*, **92**, 215 (2017)
60. K.Schmoltner, J.Kofler, A.Klug, E.J.W.List-Kratochvil. *Adv. Mater.*, **25**, 6895 (2013)
61. M.Di Lauro, S.Casalini, M.Berto, A.Campana, T.Cramer, M.Murgia, M.Geoghegan, C.A.Bortolotti, F.Biscarini. *ACS Appl. Mater. Interfaces*, **8**, 31783 (2016)
62. A.U.Alam, Y.Qin, S.Nambiar, J.T.W.Yeow, M.M.R.Howlader, N.X.Hu, M.J.Deen. *Prog. Mater. Sci.*, **96**, 174 (2018)
63. F.Buth, D.Kumar, M.Stutzmann, J.A.Garrido. *Appl. Phys. Lett.*, **98**, 2009 (2011)
64. M.E.Roberts, S.C.B.Mannsfeld, M.L.Tang, Z.Bao. *Chem. Mater.*, **20**, 7332 (2008)
65. J.Borges-González, C.J.Kousseff, C.B.Nielsen. *J. Mater. Chem. C*, **7**, 1111 (2019)
66. A.Giovannitti, C.B.Nielsen, D.T.Sbircea, S.Inal, M.Donahue, M.R.Niazi, D.A.Hanifi, A.Amassian, G.G.Malliaras, J.Rivnay, I.McCulloch. *Nat. Commun.*, **7**, 1 (2016)
67. D.A.Bernards, G.G.Malliaras, G.E.S.Toombes, S.M.Gruner. *Appl. Phys. Lett.*, **89**, 053505 (2006)
68. C.Liao, F.Yan. *Polym. Rev.*, **53**, 352 (2013)
69. H.Sirringhaus, P.J.Brown, R.H.Friend, M.M.Nielsen, K.Bechgaard, B.M.W.Langeveld-Voss, A.J.H.Spiering, R.A.J.Janssen, E.W.Meijer, P.Herwig, D.M.de Leeuw. *Nature (London)*, **401**, 685 (1999)

70. N.E.Persson, P.H.Chu, M.McBride, M.Grover, E.Reichmanis. *Acc. Chem. Res.*, **50**, 932 (2017)
71. F.Buth, A.Donner, M.Sachsenhauser, M.Stutzmann, J.A.Garrido. *Adv. Mater.*, **24**, 4511 (2012)
72. H.Schamoni, S.Noever, B.Nickel, M.Stutzmann, J.A.Garrido. *Appl. Phys. Lett.*, **108**, 073301 (2016).
73. W.Lövenich. *Polym. Sci., Ser. C*, **56**, 135 (2014)
74. K.Wijeratne, U.Ail, R.Brooke, M.Vagin, X.Liu, M.Fahlman, X.Crispin. *Proc. Natl. Acad. Sci. USA*, **115**, 11899 (2018)
75. F.X.Werkmeister, T.Koide, B.A.Nickel. *J. Mater. Chem. B*, **4**, 162 (2016)
76. H.Toss, C.Suspène, B.Piro, A.Yassar, X.Crispin, L.Kergoat, M.C.Pham, M.Berggren. *Org. Electron.*, **15**, 2420 (2014)
77. M.Magliulo, B.R.Pistillo, M.Y.Mulla, S.Cotrone, N.Ditaranto, N.Cioffi, P.Favia, L.Torsi. *Plasma Proc. Polym.*, **10**, 102 (2013)
78. H.Sinno, H.T.Nguyen, A.Hägerström, M.Fahlman, L.Lindell, O.Coulembier, P.Dubois, X.Crispin, I.Engquist, M.Berggren. *Org. Electron.*, **14**, 790 (2013)
79. R.Porrazzo, A.Luzio, S.Bellani, G.E.Bonacchini, Y.Y.Noh, Y.H.Kim, G.Lanzani, M.R.Antognazza, M.Caironi. *ACS Omega*, **2**, 1 (2017)
80. H.Sun, M.Vagin, S.Wang, X.Crispin, R.Forchheimer, M.Berggren, S.Fabiano. *Adv. Mater.*, **30**, 1704916 (2018)
81. N.Wang, Y.Liu, Y.Fu, F.Yan. *ACS Appl. Mater. Interfaces*, **10**, 25834 (2018)
82. M.Giordani, M.Berto, M.Di Lauro, C.A.Bortolotti, M.Zoli, F.Biscarini. *ACS Sensors*, **2**, 1756 (2017)
83. F.Leonardi, A.Tamayo, S.Casalini, M.Mas-Torrent. *RSC Adv.*, **8**, 27509 (2018)
84. A.S.Sizov, E.V.Agina, S.A.Ponomarenko. *Russ. Chem. Rev.*, **88**, 1220 (2019)
85. R.A.Picca, K.Manoli, E.Macchia, A.Tricase, C.Di Franco, G.Scamarcio, N.Cioffi, L.Torsi. *Ftont. Chem.*, **7**, 667 (2019)
86. F.Dinelli, M.Murgia, P.Levy, M.Cavallini, F.Biscarini, D.M.De Leeuw. *Phys. Rev. Lett.*, **92**, 90 (2004)
87. M.J.Spijkman, J.J.Brondijk, T.C.T.Geuns, E.C.P.Smits, T.Cramer, F.Zerbetto, P.Stoliar, F.Biscarini, P.W.M.Blom, D.M.De Leeuw. *Adv. Funct. Mater.*, **20**, 898 (2010)
88. A.Loi, I.Manunza, A.Bonfiglio. *Appl. Phys. Lett.*, **86**, 103512 (2005)
89. A.Caboni, E.Orgiu, M.Barbaro, A.Bonfiglio. *IEEE Sens. J.*, **9**, 1963 (2009)
90. R.F.De Oliveira, S.Casalini, T.Cramer, F.Leonardi, M.Ferreira, V.Vinciguerra, V.Casuscelli, N.Alves, M.Murgia, L.Occhipinti, F.Biscarini. *Flex. Print. Electron.*, **1**, 025006 (2016)
91. J.Kofler, K.Schmoltner, E.J.W.List-Kratochvil. *Proc. SPIE 9185. Organic Field-Effect Transistors XIII; and Organic Semiconductors in Sensors Bioelectronics VII*. 91851U (2014)
92. S.Y.Lee, G.R.Choi, H.Lim, K.M.Lee, S.K.Lee. *Appl. Phys. Lett.*, **95**, 013113 (2009)
93. H.Sirringhaus. *Adv. Mater.*, **21**, 3859 (2009)
94. D.K.Hwang, C.Fuentes-Hernandez, J.Kim, W.J.Potscavage, S.J.Kim, B.Kippelen. *Adv. Mater.*, **23**, 1293 (2011)
95. P.A.Bobbert, A.Sharma, S.G.J.Mathijssen, M.Kemerink, D.M.De Leeuw. *Adv. Mater.*, **24**, 1146 (2012)
96. L.Kergoat, N.Battaglini, L.Miozzo, B.Piro, M.C.Pham, A.Yassar, G.Horowitz. *Org. Electron.*, **12**, 1253 (2011)
97. S.Y.Lee, S.K.Lee, H.Lim, G.R.Choi. *J. Korean Phys. Soc.*, **57**, 1416 (2010)
98. *Compendium of Chemical Terminology. IUPAC Recommendation*. (Eds A.D.McNaugt, A.Wilkinson). International Union of Pure and Applied Chemistry Compendium of Chemical Terminology, 2012
99. S.Casalini, A.C.Dumitru, F.Leonardi, C.A.Bortolotti, E.T.Herruzo, A.Campana, R.F.de Oliveira, T.Cramer, R.Garcia, F.Biscarini. *ACS Nano*, **9**, 5051 (2015)
100. M.Y.Mulla, P.Seshadri, L.Torsi, K.Manoli, A.Mallardi, N.Ditaranto, M.V.Santacroce, C.Di Franco, G.Scamarcio, M.Magliulo. *J. Mater. Chem. B*, **3**, 5049 (2015)
101. G.Z.Yang. *Implantable Sensors and Systems: from Theory to Practice*. (Cham; Springer, 2018)
102. C.J.Bettinger, Z.Bao. *Polym. Int.*, **59**, 563 (2010)
103. N.Lago, A.Cester. *Appl. Sci.*, **7**, 1292 (2017)
104. L.Li, S.Wang, Y.Xiao, Y.Wang. *Trans. Tianjin Univ.*, 1 (2020)
105. C.A.Hunter, S.A.Jones. *Nat. Immunol.*, **16**, 448 (2015)
106. J.Sun, Y.Liu, S.Lv, Z.Huang, L.Cui, T.Wu. *Electroanalysis*, **28**, 439 (2016)
107. E.Stern, R.Wagner, F.J.Sigworth, R.Breaker, T.M.Fahmy, M.A.Reed. *Nano Lett.*, **7**, 3405 (2007)
108. S.Black, I.Kushner, D.Samols. *J. Biol. Chem.*, **279**, 48487 (2004)
109. H.Ohshima. *Sci. Technol. Adv. Mater.*, **10**, 063001 (2009)
110. K.Makino, H.Ohshima. *Sci. Technol. Adv. Mater.*, **12**, 023001 (2011)
111. P.Gründler. *Chemical Sensors — an Introduction for Scientists and Engineers*. (Berlin, Heidelberg: Springer-Verlag, 2007)
112. J.Kofler, K.Schmoltner, A.Klug, E.J.W.List-Kratochvil. *Appl. Phys. Lett.*, **104**, 193305 (2014)
113. X.J.Liu, B.Peng, F.Liu, Y.Qin. *Sens. Actuators B*, **125**, 656 (2007)
114. K.Schmoltner, J.Kofler, A.Klug, E.J.W.List-Kratochvil. *Proc. SPIE 8831. Organic Field-Effect Transistors XII; and Organic Semiconductors in Sensors and Bioelectronics VI,* 88311N (2013)
115. V.F.Traven, D.A.Cheptsov. *Russ. Chem. Rev.*, **89**, 713 (2020)
116. Z.Wang, J.H.Lee, Y.Lu. *Chem. Commun.*, 6005 (2008)
117. A.Chva, E.Madara. *J. Neurosci. Res.*, **1617**, 1606 (2007)
118. A.Shehu, S.D.Quiroga, P.D'Angelo, C.Albonetti, F.Borgatti, M.Murgia, A.Scorzoni, P.Stoliar, F.Biscarini. *Phys. Rev. Lett.*, **104**, 246602 (2010)
119. G.Wu, P.Feng, X.Wan, L.Zhu, Y.Shi, Q.Wan. *Sci. Rep.*, **6**, 1 (2016)
120. Y.Vlasov, A.Legin, A.Rudnitskaya, C.Di Natale, A.D'Amico. *Pure Appl. Chem.*, **77**, 1965 (2005)
121. M.Podrazka, E.Báczyńska, M.Kundys, P.S.Jeleń, E.W.Nery. *Biosensors*, **8**, 3 (2017)
122. F.P.A.Cabral, B.B.Bergamo, C.A.R.Dantas, A.Riul, J.A.Giacometti. *Rev. Sci. Instrum.*, **80**, 2 (2009)
123. C.Medina-Plaza, J.A.de Saja, M.L.Rodriguez-Mendez. *Biosens. Bioelectron.*, **57**, 276 (2014)
124. L.Lvova. In *Electronic Noses and Tongues in Food Science*. Ch. 15. (Elsevier , 2016) P.151; DOI: 10.1016/b978-0-12-800243-8.00015-9
125. A.Poghossian, H.Geissler, M.J.Schöning. *Biosens. Bioelectron.*, **140**, 111272 (2019)
126. M.Gutiérrez, A.Llobera, A.Ipatov, J.Vila-Planas, S.Mínguez, S.Demming, S.Büttgenbach, F.Capdevila, C.Domingo, C.Jiménez-Jorquera. *Sensors*, **11**, 4840 (2011)
127. M.Kundys, P.S.Jele, M.Podra, E.W.Nery. *Biosensors*, **8**, 1 (2018)
128. P.Abgrall, A.M.Gué. *J. Micromech. Microeng.*, **17**, R15 (2007)
129. A.N.Solodukhin, Y.N.Luponosov, M.I.Buzin, S.M.Peregudova, E.A.Svidchenko, S.A.Ponomarenko. *Mendeleev Commun.*, **28**, 415 (2018)
130. F.V.Drozdov, Y.N.Luponosov, E.A.Svidchenko, S.M.Peregudova, P.V.Dmitryakov, S.N.Chvalun, S.A.Ponomarenko. *Mendeleev Commun.*, **29**, 561 (2019)
131. A.N.Solodukhin, Y.N.Luponosov, A.L.Mannanov, P.V.Dmitryakov, S.M.Peregudova, S.N.Chvalun, D.Y.Parashchuk, S.A.Ponomarenko. *Mendeleev Commun.*, **29**, 385 (2019)
132. K.P.Trainov, R.F.Salikov, Y.N.Luponosov, P.S.Savchenko, A.L.Mannanov, S.A.Ponomarenko, D.N.Platonov, Y.V.Tomilov. *Mendeleev Commun.*, **29**, 304 (2019)